

# Photographic response to x-ray irradiation. I: Estimation of the photographic error statistic and development of analytic density-intensity equations

C. T. Chantler

Formulations for specular optical density as a function of incident x-ray intensity are shown to be inadequate, theoretically and compared with available data. Approximations assuming low intensities, grain densities, or energies yield significant error in typical emulsions. Unjustifiable simplifications limit analysis and consequent results. The avoidance of assumptions leads to models for rough and smooth emulsion surfaces, which correspond to Kodak 101-01 and DEF-392 emulsion types. The self-consistent use of spherical grains yields scaling that is dependent on emulsion roughness. We obtained improvement over standard formulations, avoiding the empirical character of earlier models and associated parameterization. The correlation of grain locations and occluded emulsion area is approximated within monolayer depths but neglected between layers. Effects of the incident angle from a broad source, scattering, and photoelectrons are considered. The models presented herein apply to the vacuum UV and x-ray energies from 9 eV to 20 keV and may be preferred over alternative models at lower energies, densities greater than unity, emulsions with high grain fractions, or where interpolation over energy ranges is desired. Error contributions may be dominated by intensity statistics or densitometry statistics. Both are inadequate in medium-density regimes. We have derived estimates including pseudo-binomial grain development statistics, using a summation over layers.

## 1. Introduction and Article Structure

The photographic detection of x rays in a wavelength-dispersive spectrometer can lead to resolutions that are greater than those in most electronic detection systems. This 1–3- $\mu\text{m}$  resolution in two dimensions provides a maximum amount of useful information, especially for signals of low flux or in accelerator-based or high-temperature plasma facilities where periods of observation are restricted. The treatment of certain systematics in the derivation of precision results requires this two-dimensional character, sensitivity, and resolution.

Detection systems generally provide systematic shifts, broadening, and a nonlinearity of response.

Shifts and broadening introduced by the use of photographic detection are particularly simple, but complexities arise in the nonlinearity of the response of various emulsions to radiation of different wavelengths incident at different angles to the film.

Detailed studies have been made by several authors, who fitted semiempirical formulas to measured data in controlled experiments.<sup>1–11</sup> Although these reproduce local features of the density-intensity curve, the parameters are of little physical significance, and extrapolation to other energies, densities, angles, or emulsions is uncertain and generally invalid. Knowledge of this curve is required for the correct linearization of photographic density and hence for valid absolute and relative intensities of spectral features. These in turn yield information on scattering processes and experimental parameters.

Linearized spectral profiles may be fitted with least-squares techniques to yield centroid and width estimates. Such fitting routines often assume a normal distribution of errors and noise. This is adequate for some purposes, but the resulting fitting uncertainties are distorted by this assumption. For best results and error estimates, a photographic error

---

When this work was performed the author was with Clarendon Laboratory, University of Oxford, Parks Road, Oxford OX1 3PU, England. The author is now with Quantum Metrology Division, National Institute of Standards and Technology, Gaithersburg, Maryland 20899.

Received 26 November 1991.

0003-6935/93/132371-27\$05.00/0.

© 1993 Optical Society of America.

statistic should be defined and used in further analysis.

In Section 2 we introduce variables and assumptions of the standard thick emulsion model of Henke *et al.*,<sup>8</sup> the more general and appropriate model of these authors, although they are recast slightly with a view to development and investigation of assumptions later in this and succeeding papers. In the next section the problem of statistical uncertainty presented by the definition of granularity is introduced. The three components of a solution to this are presented in Sections 3–5, with the variables involved identified therein, and caveats are presented in Section 6. This provides a framework for deriving the error statistic.

In Section 7 we then return to the thick emulsion model to identify energy regimes where stated assumptions are likely to fail or to require reinterpretation. Other assumptions are limited to low grain packing densities or low optical densities, as indicated in Section 8 and illustrated by particular characteristic  $D-I$  curves. This prepares the way for the development of the integral formulation model, beginning in Section 9, which is the main mathematical contribution of this paper and avoids some of the assumptions just indicated. Two expansions are presented that yield basic model equations presented in Section 11.

The model relies on accurate attenuation coefficients. The limitations of common tabulations for homogeneous values, and methods for partial correction of these (used herein), are presented in Section 12. The emulsion structure leading to the heterogeneous coefficient is introduced and used in Sections 13 and 14. Although the first part of these sections is mainly a summary of previously known results, they are critiqued and developed in the later part. Silver bromide clusters are assumed to be spherical, of a uniform mean diameter, and randomly distributed within the available volume, as opposed to aligned cube models.

The concept of near-spherical grains is shown to affect not only this coefficient, but in Section 15 it has a dramatic and complex effect on the basic equations of the standard thick emulsion model and on the current integral formulation. This is significantly dependent on the surface of the emulsion, characterized herein by smooth or rough extremes and a simpler “intermediate” level. The form and detail of these corrections are illustrated as a second significant modeling development. Initial layers involve a gelatin attenuation coefficient rather than the heterogeneous value.

In the remaining sections we compare the models and formulas developed with the standard thick emulsion model, noting, first, theoretical limitations of the forms, particularly of the earlier method (Section 16); second, the comparison to data in the literature for DEF-392, which is a smooth, thick, well-packed emulsion extreme; and third, the comparison with data for 101 film, which is a rough, thin, highly packed extreme. These two emulsions are

used in the experiments referred to above. The current paper is concerned primarily with specular optical density. In Section 17 observations are made of the conversion of diffuse to specular density, which is a correction of some earlier procedures. The comparison with literature in Sections 17 and 18 is confined to normal-incidence geometries. In Section 19 we indicate the expected nature of the response as a function of the angle of incidence; it is considered further in the third paper of this series. Finally, in Section 20 are comments on the improved agreement with experiment and the more physical nature of the parameters from this integral model. Difficulties are also summarized, particularly those arising from the correlation of coverage and attenuation coefficients with exposure and emulsion depth, as discussed in a succeeding paper.

## 2. Thick Emulsion Form and Parameters

Kodak DEF-392 is a thick double-sided emulsion with a heterogeneous system of AgBr grains embedded in a gelatin base and a gelatinlike supercoat. Scanning electron microscopy and  $\text{CuK}\alpha$  (8050-eV) transmission measurements yielded estimated emulsion-plus-supercoat and polyester substrate thicknesses of  $T + t_0 \approx 14.0 \pm 0.5 \mu\text{m}$  and  $t_b \approx 185 \mu\text{m}$ , a mean AgBr grain diameter  $\bar{d} \approx 1.6 \pm 0.3 \mu\text{m}$  and a mean volume fraction of AgBr grains in the emulsion of  $\%v/v \approx 0.40 \pm 0.025$ .<sup>8</sup> The last value is directly correlated with an assumed uncertainty of 6% in the determination of  $T \approx 13 \mu\text{m}$  and an assumption of the form of the effective absorption coefficient (Section 14). The supercoat thickness  $t_0$  is not determined; thus modeling of experimental transmission at lower energies is required. Other authors<sup>11</sup> report similar parameters, with  $T + t_0 \approx 14.3 \mu\text{m}$ ,  $\%v/v$  derived from transmission measurements, unchanged,  $t_b \approx 177.6 \mu\text{m}$ ,  $t_0 \approx 0.4\text{--}1.8 \mu\text{m}$ , and  $\bar{d}$  estimated to be  $1.6 \mu\text{m}$  from a range of  $1.0\text{--}1.8 \mu\text{m}$ .

The emulsion is assumed to be uniform and of average thickness  $T$ , and the absorption of a single photon is assumed to be sufficient to render a grain developable in the energy region of concern (100 eV to 20 keV). Assumptions of the standard thick emulsion model are indicated in Fig. 1. Grains are assumed to be approximately spherical with cross sec-

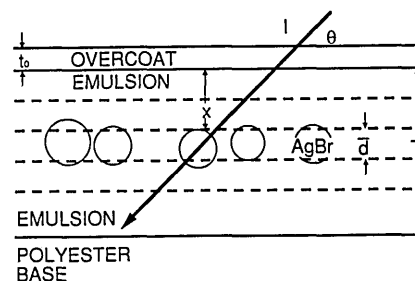


Fig. 1. Thick emulsion model for an overcoat of thickness  $t_0$  and a volume fraction  $\%v/v$  of spherical AgBr grains (of mean thickness  $\bar{d}$ ) in the gelatin emulsion at a depth  $x$ ;  $\theta$  is the angle of incidence.

tion  $\sigma$ . The probability that an individual AgBr grain of thickness  $\bar{d}$  beginning at depth  $x$  in the emulsion will absorb a photon under an exposure of intensity  $I \ll 1$  photons/ $\mu\text{m}^2$  is

$$z = I\sigma[1 - \exp(-\mu_1 d')] \exp(-\mu'x/\sin \theta - \mu_0 t_0/\sin \theta) \\ = \sigma\beta I \exp(-\mu'x/\sin \theta), \quad (1)$$

where  $d'$  is the mean path length through the grain,  $\mu_0$  and  $\mu_1$  are the gelatin and AgBr linear absorption coefficients, and  $\mu'$  is that of the heterogeneous emulsion. The integration over intensity leads to an expression, which is valid for all  $I$ , for the number of grains per unit area (in the monolayer) rendered developable by the exposure

$$M_l = M_0 P_l, \quad P_l = [1 - \exp(-z)]. \quad (2)$$

Development reduces the exposed grains to silver clusters of increased average cross section  $S$ . For nonoverlapping grains within the monolayer (and total absorption at optical frequencies in the silver grains), the fraction of light occluded by the clusters in the monolayer is given by  $\tau_l = 1 - M_l S = 1 - M_0 S [1 - \exp(-z)]$ .

The probability for shadowing (developed grains overlapping in the densitometer light beam) is assumed to be negligible, valid for small values of  $M_l S$  and  $d$ . The total optical transmission for the thick emulsion may then be given as the product of monolayer-section transmissions. Thus the density is

$$D = \log_{10}(1/\tau) = - \sum_{l=1}^{\text{Int}(T/\bar{d})} \log_{10} \tau_l = \frac{-1}{2.30} \sum_{l=0}^{\text{Int}(T/\bar{d})-1} \ln(1 - M_0 S \{1 - \exp[-\sigma\beta I \exp(-\mu' l \bar{d}/\sin \theta)]\}) \quad (3a)$$

$$\approx \frac{1}{2.30} \sum_{l=0}^{\text{Int}(T/\bar{d})-1} M_0 S \{1 - \exp[-\sigma\beta I \exp(-\mu' l \bar{d}/\sin \theta)]\}, \quad (3b)$$

where  $\beta = [1 - \exp(-\mu_1 d')] \exp(-\mu_0 t_0/\sin \theta)$ , with the assumption that  $M_l S$  is small in the last step; in the limit of thick emulsions this may be reexpressed as an integral:

$$D = \frac{1}{2.30} \int_0^{x_{\max}} N_0 S \{1 - \exp[-\sigma\beta I \exp(-\mu'x/\sin \theta)]\} dx, \quad (4)$$

where  $N_0$  is the number of grains per unit volume ( $M_0/\bar{d}$ ) and  $x = l\bar{d}$ . The assumptions of Eqs. (3b) and (4) are acknowledged by Henke *et al.*<sup>6</sup> to be too restrictive. These authors introduced an empirical scaling constant  $d_0$ , replaced  $\sigma$  and  $M_0 S$  with two parameters  $a$  and  $b$ , and replaced the integral by the

simplest form with correct limiting behavior. With  $x_{\max} = T$  (see Section 15), this gave

$$\alpha = 1 / \left( \frac{\sin \theta}{\mu'} + d_0 \right), \quad (5)$$

$$\alpha D = a \ln \left[ \frac{1 + b\beta I}{1 + b\beta I \exp(-\mu'T/\sin \theta)} \right], \quad (6)$$

$$I = \frac{1}{b\beta} \frac{\exp(\alpha D/a) - 1}{1 - \exp(\alpha D/a - \mu'T/\sin \theta)}. \quad (7)$$

### 3. Granularity and Incident Photon Statistics

Reasonable uncertainties for intensities should be based on densities measured on a densitometer. Previous literature does not provide these. They derive from a Poisson distribution for the number of photons impinging on the emulsion, the idiosyncratic pseudo-binomial distribution of the number of grains in each monolayer, and the distribution of the counting statistics of the illumination in the densitometer itself.

A measure of the standard deviation is given by the granularity<sup>12</sup>  $g = (A_d)^{1/2} \sigma_D$ , where  $\sigma_D$  is the standard deviation from a uniform mean density  $D$  when a scanning area of  $A_d$   $\text{cm}^2$  is used to measure the density. Measurement of this for 101-01 emulsion with  $A_d = 100 \mu\text{m} \times 100 \mu\text{m}$  and  $40 \mu\text{m} \times 40 \mu\text{m}$  confirmed the simple result for low densities and monolayer emulsions that  $g \propto \sqrt{D}$  for  $D < 1.1$ . This region is well below saturation; yet a marked deviation

was noted for two other near-monolayer emulsions. The relation reflects the low-intensity UV/x-ray counting statistic (if it contributes a significant error) but is not useful if this error is minimal or if the useful range of density for multilayer emulsions is considered.

Poisson errors resulting from the incident number of x rays on a region of film relate to the area of film  $A_d$  observed by the densitometer (per channel) and the number incident on the emulsion surface  $N_{\text{inc}}$  rather than on any window  $N_w = I A_d$ . One may estimate the incident number of photons in the densitometer region by using Eq. (7) and by multiplying by  $A_d \exp[-(\mu_0 t_0 + \mu_w t_w)/\sin \theta]$ . The standard deviation of this value  $N_{\text{inc}}$  is  $\sqrt{N_{\text{inc}}}$ , which gives an uncertainty in the estimate of  $I$  of

$$\sigma_I(N_{\text{inc}}) = I / \sqrt{N_{\text{inc}}}. \quad (8)$$

#### 4. Grain Statistics

Following Eq. (1) for the exposed grain distribution in each monolayer, the x-ray count incident on the window  $I_p$  yields an estimated number of grains exposed as

$$\begin{aligned}
 G_i &\approx A_d \sum_{l=1}^{\text{Int}(T/\bar{d})} M_l \approx A_d \int_0^{T-\bar{d}} N_0 \\
 &\quad \times [1 - \exp[-\sigma\beta I_p/A_d \exp(-\mu'x/\sin\theta)]] dx \\
 &\approx N_0 \sigma\beta I_p \int_0^{T-\bar{d}} \exp(-\mu'x/\sin\theta) dx \\
 &= I_p b \beta N_0 \frac{\sin\theta}{\mu'} \{1 - \exp[-\mu'(T-\bar{d})/\sin\theta]\}. \quad (9)
 \end{aligned}$$

This formula is valid for low values of  $I$  and  $z$ , relatively high energies (where  $d_0$  is not significant), and uses a mean value of  $M_0/d_0 = N_0 = (\%v/v)/V_0$ , where  $V_0$  is the grain volume. It replaces  $\sigma_g = (\pi/4)\bar{d}^2$  of 2.01  $\mu\text{m}^2$  (with  $\bar{d}$  for DEF) with Henke's empirical, effective estimate<sup>8</sup> of  $b = 1.69 \mu\text{m}^2$ .

Each monolayer will follow binomial statistics in the limit of low absorption or of narrow monolayers. This may be used to derive an estimate of the grain distribution. Summing over monolayers results in this second estimate:

$$G_s = \sum_{l=0}^{\text{Int}(T/\bar{d}-1)} M_0 A_d \left\{ P_l \pm \left[ \frac{P_l(1-P_l)}{M_0 A_d} \right]^{1/2} \right\}, \quad (10a)$$

where  $M_0 \approx \bar{d}(\%v/v)/V_0$ . This should be an estimate of the density of grains with front surfaces at

---


$$\begin{aligned}
 D_G &= \frac{-1}{\ln 10} \sum_{l=0}^{\text{Int}(T/\bar{d}-0.5)} \ln \left( 1 - \frac{SG_{\text{tot}}}{A_d} [2 - \exp(-z_{2l}) - \exp(-z_{2l+1})] \right) \\
 &\quad \pm \frac{SG_{\text{tot}}}{A_d} \left\{ \frac{[1 - \exp(-z_{2l})]\exp(-z_{2l}) + [1 - \exp(-z_{2l+1})]\exp(-z_{2l+1})}{G_{\text{tot}}/2} \right\}^{1/2}, \quad (12)
 \end{aligned}$$


---

the front of the layer, since otherwise

$$\begin{aligned}
 P_l &\approx 1 - \exp(-z'), \\
 z' &= \begin{cases} z \exp(-\mu'\bar{d}/2/\sin\theta), & z > 1 \\ \frac{z}{\bar{d}} \int_{\Delta x=0}^{\bar{d}} \exp(-\mu'\Delta x/\sin\theta) \Delta x \\ = \frac{z \sin\theta}{\bar{d}\mu'} [1 - \exp(-\mu'\bar{d}/\sin\theta)], & z \leq 1. \end{cases} \quad (10b)
 \end{aligned}$$

The latter form is precise for small  $z$ , while for large  $z$  the simpler expression using  $\bar{x} \approx \bar{d}/2$  is more accurate. The second case in Eq. (10b) is required only for low energies or grazing-incidence angles.  $P_l$  is constant only when absorption is small through a single monolayer. This is why the multilayer development was replaced by an integral in Eq. (4) and why Eq. (3) is erroneous. For the current error analysis, each monolayer may be divided into one, two, or more parts, where the number of grains in each will be given to increasingly accurate precision by  $A_d/(M_0)$ ,  $A_d/(2M_0), \dots$ , and the assumption of constant  $P_l$  becomes more valid. For the use of two sections this gives

$$\begin{aligned}
 G_s &= G_{\text{tot}} \sum_{l=0}^{\text{Int}(2T/\bar{d}-1)} \left( [1 - \exp(-z)] \right. \\
 &\quad \left. \pm \left\{ \frac{[1 - \exp(-z)]\exp(-z)}{G_{\text{tot}}} \right\}^{1/2} \right) \\
 &= G_{\text{tot}} \left\{ \sum_{l=0}^{\text{Int}(2T/\bar{d}-1)} [1 - \exp(-z)] \right\} \\
 &\quad \pm \left\{ G_{\text{tot}} \sum_{l=0}^{\text{Int}(2T/\bar{d}-1)} [1 - \exp(-z)]\exp(-z) \right\}^{1/2}, \quad (11) \\
 G_{\text{tot}} &= \frac{\bar{d} \%v/v}{2 V_0} A_d,
 \end{aligned}$$

with  $G_{\text{tot}}$  the total number of grains whose front surfaces lie in each segment.

The summation of errors in quadrature is common to Gaussian and Poisson statistics but requires independence of terms; this is valid for one section but increasingly invalid for multiple  $A_d/(nM_0)$  sections per monolayer (especially with regard to densities). It is an adequate approximation for the binomial distribution with two sections. The consequent error in density, when Eq. (3a) is used, may be estimated from

where  $\sigma_g$  may be used as an approximation to  $S$ , the Ag cluster size on development. For low energies  $z$  should be replaced by  $z'$  modified from Eq. (10b). This formula assumes a negative correlation between the locations of grains at different depths in a given monolayer, beyond which correlation is assumed to be negligible. It neglects negative correlation between the second segment of one monolayer and the first of the next monolayer, which can be significant. One may relate the error in density directly to grain statistics by using the error for a given monolayer  $\sigma(D_{2l})$  and the estimated number of grains exposed

per monolayer  $G_{2l}$ :

$$\sigma_D(\text{grain}) = \left[ \sum_{i=0}^{\text{Int}(T/\bar{d}-0.5)} \sigma(D_{2l})^2 \right]^{1/2}, \quad (13)$$

$$\begin{aligned} \sigma(D_{2l}) &= \frac{\delta D_G}{\delta G_{2l}} \sigma(G_{2l}) \\ &= (2G_{\text{tot}})^{1/2} \{ [1 - \exp(-z_{2l})] \exp(-z_{2l}) \\ &\quad + [1 - \exp(-z_{2l+1})] \exp(-z_{2l+1}) \}^{1/2} \\ &\quad \times \frac{S/A_d}{\left(1 - \frac{SG_{2l}}{A_d}\right) \ln 10}, \end{aligned} \quad (14a)$$

$$G_{2l} = G_{\text{tot}} [2 - \exp(-z_{2l}) - \exp(-z_{2l+1})]. \quad (14b)$$

## 5. Densitometer Photon Counting Statistics

Variations in (visible photon) counting statistics with density occur in the densitometer detector. The need for automation and stability of the illuminating source requires that the densitometer lamp voltage and current be held constant, stabilized, and invariant. The density error in the densitometer caused by counting statistics is

$$\sigma_D(I_{\text{det}}) = \frac{1/\sqrt{I_{\text{det}}}}{\ln 10} \quad (15)$$

from  $D = -\log_{10}[(I_{\text{det}} \pm \sqrt{I_{\text{det}}})/I_0]$ . Earlier densitometry of photographic spectra at Oxford (and elsewhere) scanned each channel of data for 1 s regardless of the density (and the detected photon frequency).<sup>13-15</sup> The lamp was set to give 26 kHz at background densities (near the maximum permitted by the Oxford control system), so that the detector count  $I_{\text{det}}$  was

$$I_{\text{det}} = 26,000 \times 10^{-D}. \quad (16a)$$

We normalized this form of error by counting for longer times according to the density observed. Densitometry counting for  $\sim 26,000$  counts, up to a maximum of 310.5 s/channel, gives a relatively uniform and low counting error, especially for densities of  $< 2.6$ . We achieved this by counting for 0.5 s to gain an estimate of the time required to accumulate 26,000 counts, followed by the remainder. An upper limit of 310 s/channel prevents low counts in the 0.5-s test from leading to excessively long counting times, stalling the program, and possibly permitting thermal fluctuations of the apparatus with time to affect measurements. Densities up to 6.2 may be measured with uncertainties from the 310-s counting limit. This is relatively slow, but it minimizes variance, giving

$$I_{\text{det}} \approx \begin{cases} 26,000, & D \leq 2.5, \\ 8073 \times 10^{3-D}, & 6.2 > D > 2.5. \end{cases} \quad (16b)$$

In Fig. 2 are plots of the density and density errors for DEF emulsion with Eqs. (12), (15), and (16) as a function of  $\log(\text{intensity})$  and energy, with parameters from the *smooth* model fits of Section 17. Grain errors dominate at lower densities and are functions of detector area, assumed here to be 2500  $\mu\text{m}^2$ . Grain uncertainties peak near saturation and decline rapidly (as information regarding intensity is lost). Uncertainties depend on the distribution of populations of grains in each layer, which varies with energy (Fig. 3). These grain errors follow a relatively simple model, which appears to fail at higher energies, so may be inaccurate by a factor of 2. At lower energies model-based oscillations from the finite layer summation become significant. Detector statistics rise dramatically above  $D \approx 7.0$ , as densitometer counts per channel fall below unity. Increasing the flux or counting times (as in other densitometry systems) to, e.g.,  $I_{\text{det}} = 10^{9-D}$ , can be useful in narrow density ranges.

Results are somewhat different for 101 emulsions (Fig. 4). This represents the thin emulsion extreme, which is estimated<sup>6,11</sup> to have  $T \approx 2 \mu\text{m}$ ,  $t_0 \approx 0 \mu\text{m}$ ,  $\bar{d} \approx 0.7-1.0 \mu\text{m}$ , while  $\%v/v$  is assumed to be near unity (see Section 8) with spaces rather than gelatin between grains. Here the *smooth* model form of Table 5 fails completely. The *rough* model form [where  $z_0 = z(x=0)$  is used for first and second half-layers] is adequate between 9 and 200 eV but fails at higher energies. Uncertainties depend on the densitometer arrangement, since detector photon counting and background uncertainty can dominate at low and high densities. Grain statistics dominate in the most useful region, where densities lie between 0.2-0.5 and 1.8. X-ray/UV counting statistics can dominate at lower energies for densities up to 0.5, if detector statistics are improved sufficiently. The energy dependence of these errors is less for this thin emulsion than for DEF (Fig. 5).

The final uncertainty in linearized incident x-ray intensity may be found when one scales  $\sigma_D(\text{grain})$ ,  $\sigma_D(I_{\text{inc}})$ , and  $\sigma_D(I_{\text{det}})$  by  $\delta I/\delta D$  using Eq. (7). Use of  $\delta I/\delta D$  in a nonlinear relation with potentially large errors may be questioned; so

$$\sigma_I = I(D \pm \sigma_D) - I(D) \quad (17)$$

may be used instead, adding errors in quadrature. Data are quoted for granularity as a function of density between  $D = 0.01$  and  $D = 1.1$  and agrees with the sum of grain and incident x-ray photon uncertainties to well within a factor of 2. The advantage of the current modeling is that results may be predicted or extrapolated to higher densities, higher energies, and other emulsions.

## 6. Optical Clustering

In developed emulsions the smallest statistical unit appears to be larger than the grain size.<sup>16</sup> Errors derived by Henke's formulation (Section 2) yield fits of peaks with  $\chi_r^2 \approx 6$  instead of the order of unity. Fitting complex profile shapes with simple forms is

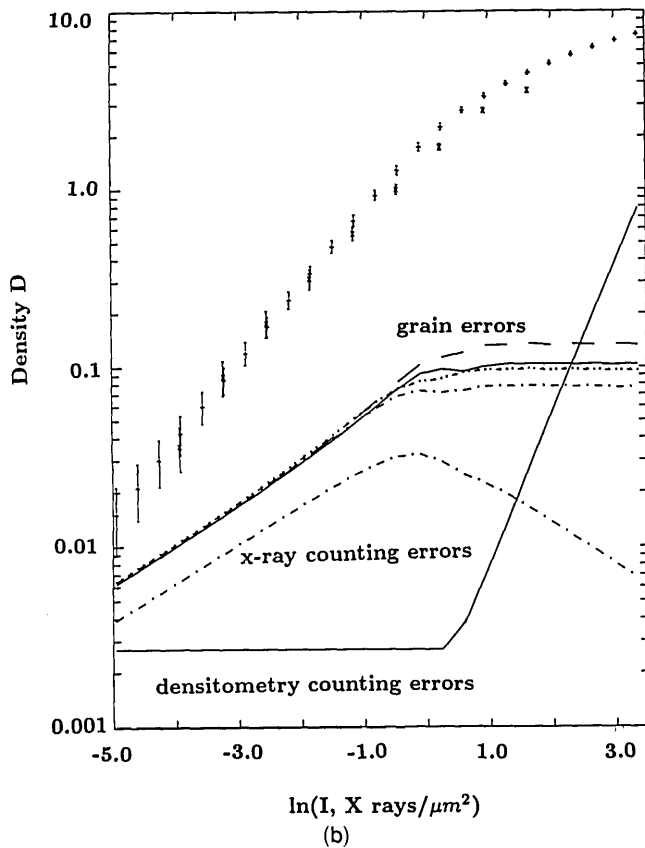
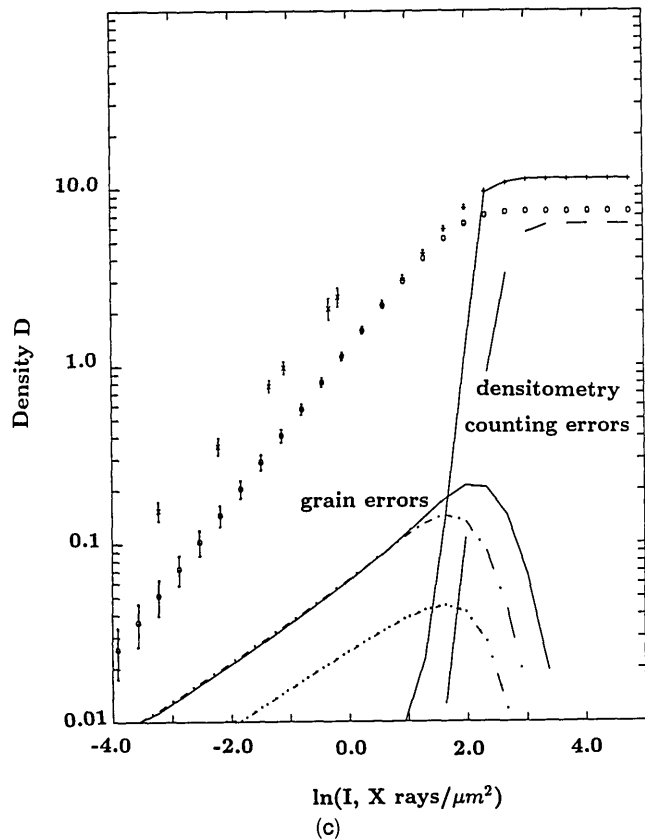
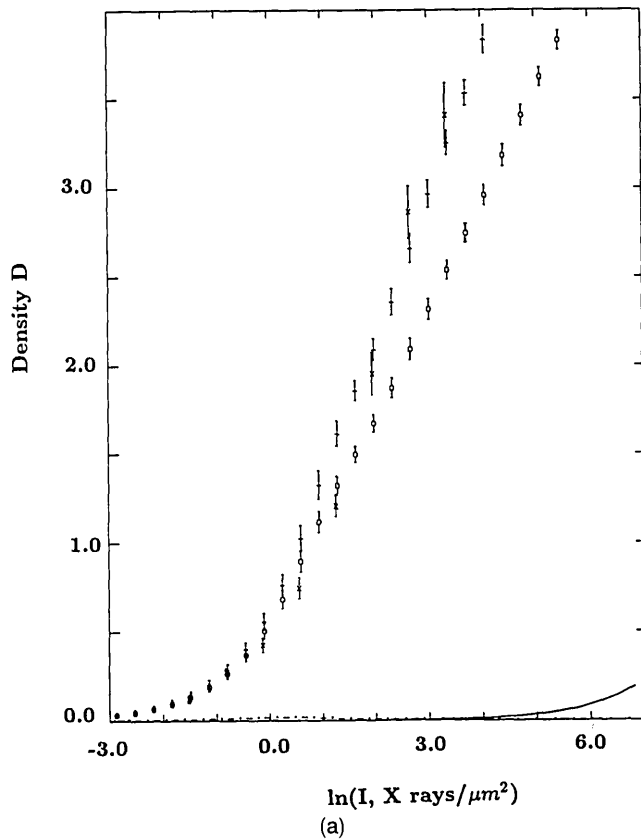


Fig. 2. Simple density estimates and density errors versus  $\ln(I)$  for DEF emulsion as described in Sections 3–5 for rough ( $\circ$ ) and smooth ( $+$ ) emulsion surface assumptions compared with experiment ( $\times$ ) for (a) 0.93 keV, (b) 1.74 keV, and (c) 8.05 keV: (a) Approach to the linear  $D - \ln I$  regime and the dominant uncertainty from grain statistics compared with densitometry counting errors (—) and Poisson x-ray counting uncertainty (·-·). (b) This becomes more apparent when a logarithmic scale for  $D$  is used and the dominance of densitometry errors for higher energies and  $D > 1$  is shown. The four curves (—, ---, ·-·, and ·-·) show rough and smooth grain error contributions with different parameter sets, as discussed in the text, indicating the insensitivity of the error to this variation. (c) Significant disagreement with experiment arises from the simple model, with rough and smooth models identical except at the saturation limits, densitometry statistics becoming serious above  $D = 6$ , and grain (—, ·-·) and x-ray (·-·) counting errors peaking and declining below saturation levels. The dashed curve assumes a much higher flux in the densitometer (see Section 5) but yields similar qualitative conclusions.

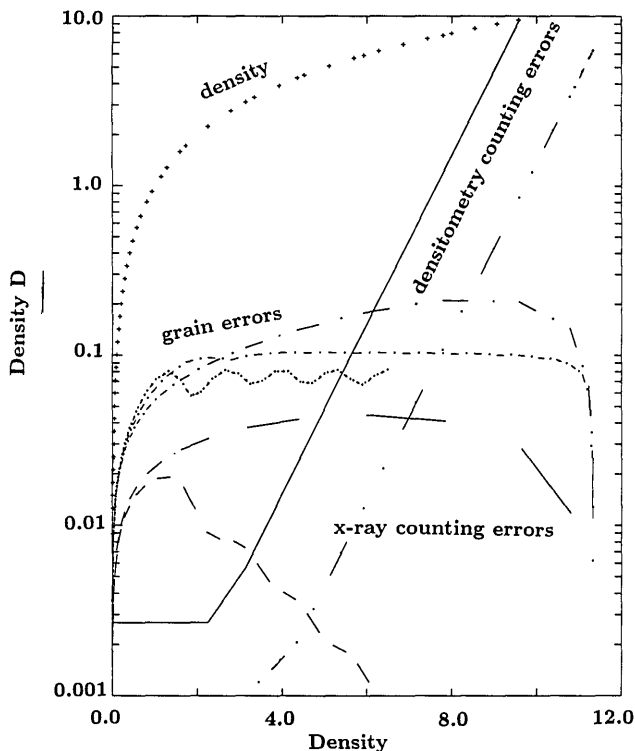


Fig. 3. Error contributions from densitometer photon statistics (—; high flux, ····), x-ray counting errors (---, high and low energies), and grain contributions (···, ···, and — for 0.93, 1.74, and 8.05 keV) to  $D$  (+) versus  $D$ , showing the dependence on energy by different layer probabilities.

partially responsible, but a contribution arises from the apparent grouping of grains. This *graininess* corresponds typically to aggregates of two to three developed grains. It becomes significant for slit sizes below  $4000 \mu\text{m}^2$ , depending on emulsion and development procedure.

This superposition of clusters as viewed by the densitometer is dominant near densities of 0.3 where half of the area is occluded. For a given exposure and a given mean number of exposed grains, the observed density follows a nearly Gaussian (but skew) distribution. For high densities this is more appropriately described by the distribution of holes than of clusters. For low (or high) densities each developed grain (or undeveloped hole) is surrounded by undeveloped (developed) grains, so that the granularity of the image is identical to that of the grains (holes). At high densities the effective hole size is reduced by shadowing from surrounding grains, so the granularity and error distribution of the image may be less than that of a grain. Densities around 0.3 yield a mean optical unit as a cluster of three to four grains separated from adjacent units. They are not true clusters, usually being overlapping grains from different layers. The limit is reached when the overlap forms a more-or-less continuous network throughout the film area, at which point the statistical description applied to the holes (Ref. 16, p. 844).

Fixing, washing, and drying have no effect on granularity (unless reticulation occurs), and underde-

velopment only affects it through the partial development of a grain giving a finer image, which is not readily amenable to theory. Optical clustering is partially accounted for in simple expressions (above) for grain errors; note that the distribution is widest when 50% of the grains in any layer are developed. Ideally the correlation of these statistical errors between layers should be included. This may yield an average increase in statistical error of a factor of 2–3 for  $D \approx 0.3$ .

## 7. Energy Regime for Models

Models of Section 2 are of limited value for visible light where three to four or more photons are required on average for a grain to be rendered developable. Reciprocity law failure, intermittency, and related effects can arise in this low-energy regime as a consequence of the required multiphoton excitation. Conversely they do not arise in the x-ray regime, and for most emulsions they are negligible for wavelengths shorter than 175 nm ( $E > 7.1 \text{ eV}$ ).<sup>12</sup> Eberhard (and Kostinsky) effects caused by the development of dense spectral lines have, however, been shown to be significant for  $D > 0.3$  and  $E < 10.4 \text{ eV}$ . The approximations given below regarding absorption coefficients become increasingly significant for energies below 50 eV or near absorption edges or resonance structures, which limits the validity of expected curves.

Soft x rays yield a latent image on grains only at *sensitivity specks*, which are commonly distributed over the surface of grains with a random (Poisson) probability of zero, one, two or more such sites per grain, depending on the sensitivity of the emulsion. Conversely higher-energy x rays are able to initiate latent images at any location in the grain. Particular grains with zero sensitivity specks may be developable only by higher-energy x rays, so that the available number of grains  $G_{\text{tot}}$  increases slightly with energy. This small effect is significant only for perfect spherical grains with low sensitivity and is neglected in the above formulas. Energies of the order of 20 keV can develop multiple grains per x ray, as excited energetic electrons or Compton-scattered photons propagate through the emulsion (Section 12).

Equation (3) treats the first layer as having  $x = 0$ , corresponding to all grains in the first monolayer being aligned and uniform, assuming that the appropriate absorption coefficient for the second monolayer is  $\mu'$ . Equation (4) allows random grain depths but assumes that  $\mu'$  is valid for the first layer, which is inadequate for low-energy photons. Low-energy x rays are equally capable of exposing grains when they are absorbed at the surface layer, compared with higher-energy rays absorbed throughout the volume. In the former extreme the absorption coefficient of the first half-layer will be  $\mu_0$  up to the grain surface and  $\mu_1$  within the grain. The attenuation of radiation prior to the grain yields

$$z = \sigma\beta I \exp(-\mu_0 x / \sin \theta) \quad (18)$$

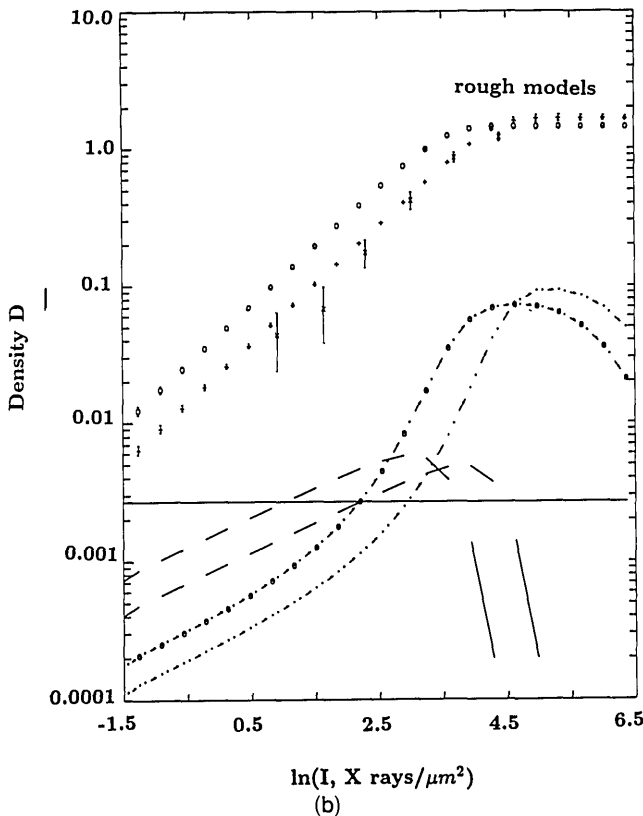
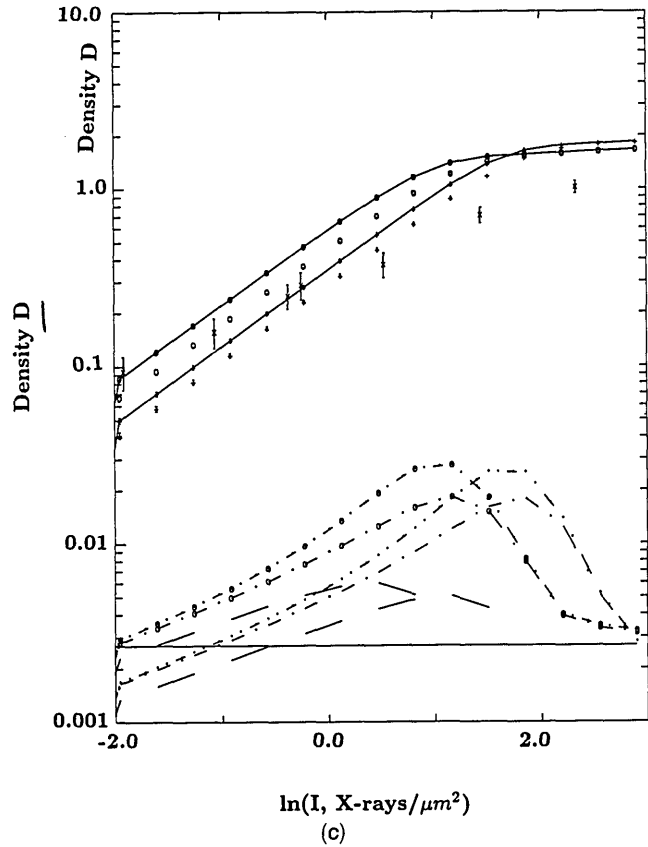
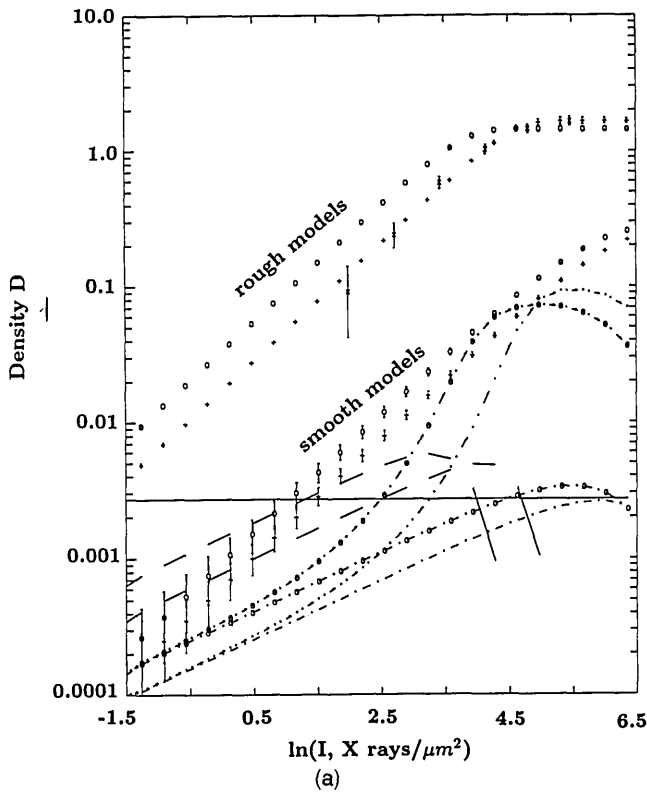


Fig. 4. Simple density estimates and density errors versus  $\ln(I)$  for 101 emulsion as described in Sections 3–5 for rough and smooth models ( $\circ$  and  $+$ ), compared with experiment ( $\times$ ) for (a) 9.508 eV, (b) 16.869 eV, and (c) 277 eV. The smooth model is indicated by the lower curves with the same symbols in (a) and (b) and by the symbols with solid curves through them in (c). The smooth model fails completely, while the rough form represented by  $+$  [where  $z_0 = z(x = 0)$  is used for the first and second half-layers] is adequate between 9 and 200 eV but fails at higher energies. The densitometry uncertainty ( $—$ ) is constant for the method described in the text for the low densities observed. Detector photon counting and background uncertainty can dominate at low and high densities.

Grain statistics ( $\circ$   $\cdots$ —,  $\cdots$ — are for rough  $\circ$  and  $+$  models and  $\circ$   $\cdots$ —,  $\cdots$ — are for smooth models) dominate between  $D \approx 0.2$ – $0.5$  and  $1.8$ . UV/x-ray counting errors ( $—$ ) can dominate at lower energies for densities up to  $0.5$ , if detector statistics are improved sufficiently.

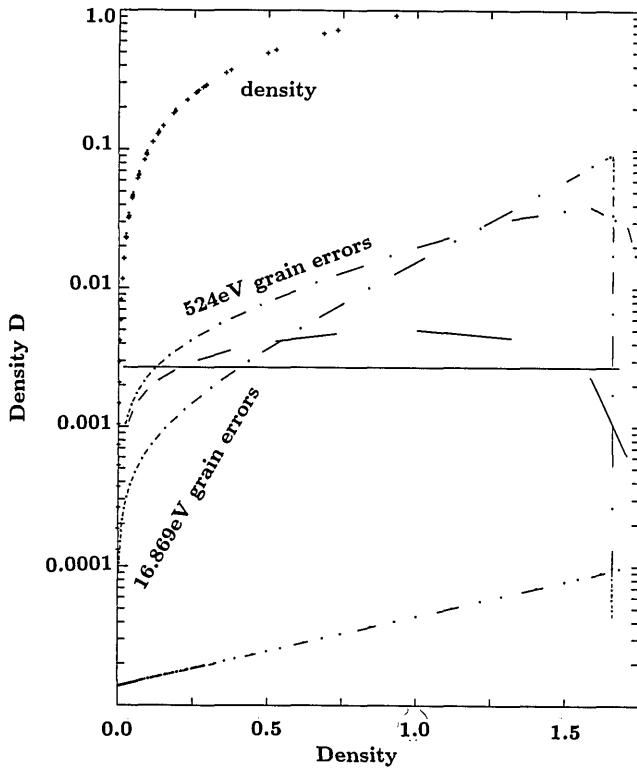


Fig. 5. Error contributions, 101 emulsion, from densitometer photon statistics (—; high flux, ···), x-ray counting errors (---), and grain contributions [—·—, smooth for higher energy (524 eV)] to  $D$  (+) versus  $D$ , showing the dependence on energy by different layer probabilities.

rather than Eq. (1). The absorption in deeper half-layers will approach the  $\mu'$  value. To first order, but avoiding reduction of the logarithm in Eq. (3a), this yields

$$D = \frac{-1}{2.30} \ln(1 - M_0 S \{1 - \exp[-\sigma\beta I \exp(-\mu_0 \bar{d}/2/\sin \theta)]\}) - \frac{1}{2.30 \bar{d}} \int_{\bar{d}}^{T-\bar{d}} \ln(1 - M_0 S \{1 - \exp[-\sigma\beta I \exp(-\mu' x/\sin \theta)]\}) dx \quad (19a)$$

instead of Eq. (3b) or (4);  $\bar{d}/2$  is a good approximation to the mean depth of the first layer for  $E \geq 1$  keV. [See also Ref. 13, Chap. 4, for the earlier development neglecting Eq. (18).] At lower energies the mean depth at which absorption occurs is  $\bar{x} = [(\sin \theta)/\mu_0] - \bar{d} \exp(-\mu_0 \bar{d}/\sin \theta) / [1 - \exp(-\mu_0 \bar{d}/\sin \theta)]$ , while the mean value of  $I \exp(-\mu_0 x/\sin \theta)$  is

$$\frac{I \sin \theta}{\mu_0 \bar{d}} [1 - \exp(-\mu_0 \bar{d}/\sin \theta)].$$

Reusing  $z$  and

$$F(z) = \frac{-1}{2.30 \bar{d}} \ln\{1 - M_0 S [1 - \exp(-z)]\}$$

allows this to be reexpressed as

$$D \approx dF[\sigma\beta I \exp(-\mu_0 \bar{d}/2/\sin \theta)] + \frac{\sin \theta}{\mu'} \int_{z_{\min}}^{z_{\max}} \frac{F(z)}{z} dz \approx \frac{\sin \theta}{\mu_0} \int_{z'_{\max}}^{\sigma\beta I} \frac{F(z)}{z} dz + \frac{\sin \theta}{\mu'} \int_{z_{\min}}^{z_{\max}} \frac{F(z)}{z} dz,$$

$$z_{\min} = \sigma\beta I \exp[-\mu'(T - \bar{d})/\sin \theta],$$

$$z_{\max} = \sigma\beta I \exp(-\mu' \bar{d}/\sin \theta),$$

$$z'_{\max} = \sigma\beta I \exp(-\mu_0 \bar{d}/\sin \theta). \quad (19b)$$

The additional contribution to the density of the first layer is of the order of 4% for 7-keV x rays; it increases to 20% for 1 keV and lower energies. The importance of this first layer versus other layers also increases with decreasing energy, depending on exposure. For 1-keV x rays and  $\sigma\beta I \leq 1$  (relatively low exposures) the overall increase is  $\sim 15\%$ . This is a partial justification for the use of the parameter  $d_0$  in Eq. (5), which reproduces to first order the effect of the initial monolayer on densities.

## 8. Packing Densities, Eq. (3b), and the Characteristic $D$ - $I$ Curve

A layer of hexagonal close-packed spherical grains of uniform size would occlude a cross-section fraction of  $M_0 \sigma_g = 90.7\%$  for normal-incidence light (in the densitometer). This packing would correspond to  $\%v/v \approx 74\%$ . Simple cubic packing would yield  $M_0 \sigma_g = 0.785$  and  $\%v/v = (\pi/6) \approx 0.524$ . DEF-392 film has a reasonably precise value of  $\%v/v \approx 0.40$ , which is the highest for the set of commercial films reported by Henke *et al.*<sup>7,8</sup> (Most have  $\%v/v \approx 0.1$ – $0.2$ .)

This and other emulsions may be modeled by loose cubic packing of spheres with some grains being smaller than average, some vacancies, and a typically small gap between adjacent spheres. DEF could be modeled on the cubic arrangement with 13% of the sites being vacant, 22% with a mean diameter  $\bar{d} \approx 0.8 h$ , and the remainder with  $\bar{d} \approx 0.98 h$ , where  $h$  is the mean separation of the centers of spheres. If grains are aligned in layers, each layer in the DEF-392 emulsions, of height  $h$ , would have  $M_0 \sigma_g \approx 1.5 [(\pi/6) (\%v/v)^2]^{1/3} \approx 0.65$ . The model in Section 2 considers the effective separation of layers to be  $h = \bar{d}$  by definition, so that each layer of height  $\bar{d}$  has  $M_0 \sigma_g \approx 1.5 (\%v/v) = 0.6$ . Electron micrographs of typical

unexposed and developed grains appear to be of similar size and shape,<sup>16</sup> so a similar model should apply to cross sections of exposed layers and silver clusters.

The assumption leading to Eqs. (3b) and (4) is that  $F(z)$  in Eq. (19a) may be represented by

$$\frac{M_0 S}{2.30 \bar{d}} [1 - \exp(-z)]$$

or that  $z \ll 1$ . This is valid for deep layers where absorption is nearly complete within the emulsion or for low exposures. Although the DEF has  $T \approx 8\bar{d}$ , this limitation is significant for medium-energy x rays. If each layer had a maximum density of 0.377 (here  $M_0 S = 0.75$ ), with an overall maximum density of  $\sim 3.05$ , this approximation would underestimate the maximum as 0.204/layer or 1.651 overall. Linearization with Eq. (3b) or (4) would fail completely at this limit.

Densities of 1.0 (or 0.123 average per layer with the first layer having  $D \approx 0.2$ ) may expose 69% of the grains in the first layer. This corresponds to  $z \approx 1.2$ , and the contribution to density would be interpreted as 0.15, an error of 25%. Only when all layers have  $D < 0.1$  (41% of the grains exposed,  $z \approx 0.53$ ) does the density error fall below 11%, while the error in linearized exposure is somewhat greater (20%).

Figure 6 shows a variety of model predictions for 8.05-keV x rays, all of which display the regimes and transition regions of the characteristic curve. Saturation occurs at the high exposure limit, yielding  $D = D_{\max}$ , independent of  $I$ . An intermediate regime follows  $D \approx a_i \log(I/I_i)$ , where  $a_i$  and  $I_i$  are constants for a given energy, film, and incident angle. This corresponds to a steady state, where upper layers are almost fully exposed and additional intensity adds exposure to deeper and deeper layers. A low-exposure regime follows  $D \approx a_l I$ , where transmission is dominated by the first layer, which is also largely unexposed. For high energies and low absorption coefficients, the range of applicability of these regimes is reduced and the transition regions become more significant.

Equations (3a), (19), and (6) all display the low-exposure, low-energy, and saturation limits but differ in evaluation of scaling constants, transition regions, and the location of the intermediate regime.

### 9. Derivation of the Integral Formulation

$y = e^{-z}$  may be introduced so that the (second) integral in approximation (19b) becomes

$$\frac{\sin \theta}{\mu'} \frac{1}{2.30 \bar{d}} \int_{\exp(-z_{\max})}^{\exp(-z_{\min})} \frac{\ln[1 - M_0 S(1 - y)]}{y \ln y} dy > 0. \quad (20)$$

If the assumption leading to Eq. (3b) is used, this simplifies to

$$-a \int \frac{1 - y}{y \ln y} dy.$$

The first term integrates to  $\ln(-\ln y)$  for  $0 < y < 1$ . This dominates over the linear portion of the  $D - \ln I$  curve. However, the second term integrates to

$$\int \frac{-dy}{\ln y} = -\ln(-\ln y) - \ln y - \frac{(\ln y)^2}{4} - \frac{(\ln y)^3}{18} - \frac{(\ln y)^4}{96} - \frac{(\ln y)^5}{5.5!} \dots, \quad (21)$$

which cancels the leading and dominant contribution, leaving the infinite series. One may expand Eq. (20), using

$$\begin{aligned} -\ln[1 - M_0 S(1 - y)] &= M_0 S(1 - y) + \frac{[M_0 S(1 - y)]^2}{2} + \dots \\ &+ \frac{[M_0 S(1 - y)]^n}{n} + \dots \end{aligned} \quad (22)$$

For  $y \approx 1$  the earlier approximation is valid, and the higher terms in Eq. (21) are negligible, while for  $M_0 S \approx 0.75$  and  $y = 0$  the first four terms in Eq. (22)

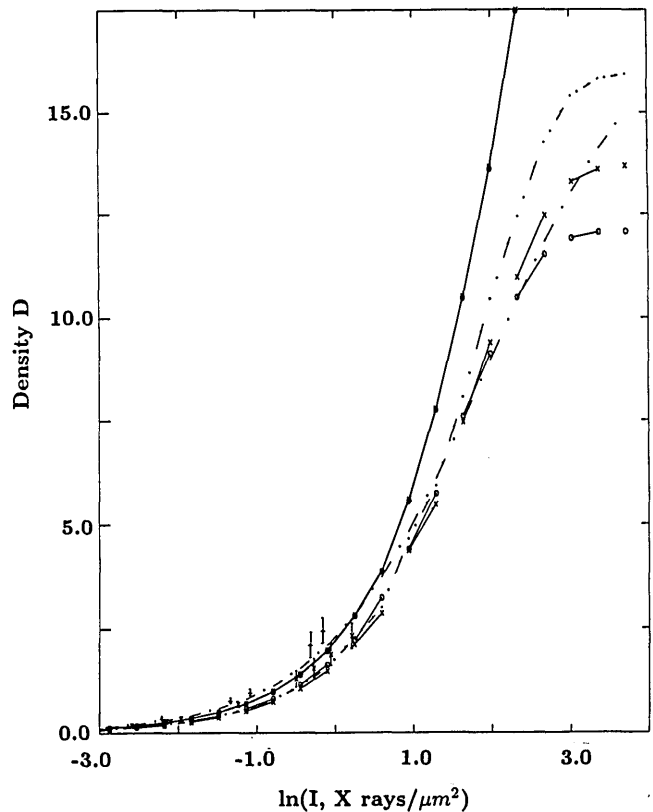


Fig. 6. Characteristic curve of density versus  $\ln I$  (for 8.05 keV). Experimental data (Henke *et al.*, +; Phillips and Phillips, x) cover only the first transition region, while all models show expected forms for the characteristic curve and agree with this low-density data. Rough and smooth surface models [—x—, —○— using Eq. (25b); x-x, ○-○ using Eqs. (25a) and (25c)] may be compared with an earlier model (---) and with an unphysical parameter set (·-·,  $T = 24 \mu\text{m}$ ) as discussed in the text. Models diverge for higher densities.

are sufficient to achieve an accuracy of 10%. It is useful to separate the coefficients of each power of  $y$  in the integrand of Eq. (20). The term  $1/(y \ln y)$  has the coefficient

$$M_0S + (M_0S)^2/2 + (M_0S)^3/3 + (M_0S)^4/4 + \dots \rightarrow -\ln(1 - M_0S) \quad (23)$$

with the first four terms providing 90% of the limiting value in the extreme just given;  $1/(\ln y)$ ,  $y/(\ln y)$ , etc. are indicated in Table 1, showing that the first four terms provide only 68% and 26% of the limiting values for  $M_0S = 0.75$ , since the convergence is nonuniform. Each coefficient increases in magnitude; thus the integral of the limit diverges. The series should therefore be truncated at a given term, which may be the fourth term (permitting an error of <10%). Exact and truncated term coefficients for two probable extreme values of  $M_0\sigma_g$  for DEF (allowing for a regular structure and packing), an intermediate value, and the general case (especially for low packing densities) are indicated in Table 1. Although convergence for the higher powers is not obtained, this is unnecessary for the convergence of the function. Equation (20) then becomes

$$\begin{aligned} & \frac{\sin \theta}{\mu' 2.30d} \\ & \times \left[ M_0S + \frac{(M_0S)^2}{2} + \frac{(M_0S)^3}{3} + \frac{(M_0S)^4}{4} \right] \\ & \times \left[ \ln z \right]_{z_{\min}}^{z_{\max}} - \frac{M_0S[1 - (M_0S)^4]}{1 - M_0S} \\ & \times \left[ \ln z - z + \frac{z^2}{4} - \frac{z^3}{18} + \frac{z^4}{96} - \frac{z^5}{5.5!} \dots \right]_{z_{\min}}^{z_{\max}} \\ & + \left[ \frac{(M_0S)^2}{2} + (M_0S)^3 + 1.5(M_0S)^4 \right] \\ & \times \left[ \ln z - z + \frac{z^2}{4} - \frac{z^3}{18} + \frac{z^4}{96} - \frac{z^5}{5.5!} \dots \right]_{2z_{\min}}^{2z_{\max}} \\ & - \left[ \frac{(M_0S)^3}{3} + (M_0S)^4 \right] \\ & \times \left[ \ln z - z + \frac{z^2}{4} - \frac{z^3}{18} + \frac{z^4}{96} - \frac{z^5}{5.5!} \dots \right]_{3z_{\min}}^{3z_{\max}} \\ & + \frac{(M_0S)^4}{4} \left[ \ln z - z + \frac{z^2}{4} - \frac{z^3}{18} + \frac{z^4}{96} - \frac{z^5}{5.5!} \dots \right]_{4z_{\min}}^{4z_{\max}} \end{aligned} \quad (24)$$

The expansion of each integral oscillates, converging quickly for low  $z$ : for  $z = 1$  ( $y = 0.368$ ) the first three terms give an error of only 6% (which is mainly equivalent to the fourth term); while for  $z = 1.386$  ( $y = 0.25$ ) the first four terms are required and give an accuracy of 4%. For thick emulsions or low

Table 1. Typical Coefficients and Series Convergence of  $-\ln[1 - M_0S(1 - y)]$

		Powers of $y$				
$M_0S$ Terms		$\frac{1}{y \ln y}$	$\frac{1}{\ln y}$	$\frac{y}{\ln y}$	$\frac{y^2}{\ln y}$	$\frac{y^3}{\ln y}$
0.75	4	1.251	-2.05	1.1777	-0.457	0.0791
0.75	$\infty$	1.386	-3.00	4.50	—	—
0.65	4	0.9974	-1.5256	0.7536	-0.2700	0.0446
0.65	$\infty$	1.050	-1.857	1.724	—	—
0.55	4	0.799	-1.110	0.455	-0.147	0.0229
0.55	$\infty$	0.799	-1.222	0.747	—	—
$x$	4	$-\ln(1-x)$	$\frac{x(x^4-1)}{1-x}$	$\frac{x^2}{2} + x^3 + \frac{3x^4}{2}$	$\frac{-x^3}{3} - x^4$	$\frac{x^4}{4}$
$x$	$\infty$	$-\ln(1-x)$	$\frac{-x}{1-x}$	$\frac{x^2}{2(1-x)^2}$	—	—

photon energies, the lower limit of  $z$  is given by the first three terms (for each integral).

In a weak background exposure all five  $z$  expansions in Eq. (24) are dominated by the first term; but these nearly cancel, so that the second ( $z$ ) term is needed. The third term ( $z^2/4$ ) is required to give the necessary convergence of each integral expansion but gives a negligible overall contribution for  $4z < 0.693$ . All five expansions are essential, with the last contributing up to 50% of the final value (because the sequence oscillates). Here  $y > 0.5$  so further contributions following Eq. (22) are negligible.

For integrations over  $z > 2.9957$  ( $y < 0.05$ ) the first integral alone gives an accuracy of 96%. This corresponds to large densities and high-energy photons and yields the linear region of the  $D - \ln I$  curve. The expansion neglects terms of order  $(M_0S)^5$  and higher, so that the limit when  $y \rightarrow 0$  can underestimate the final result by 5–10% for  $M_0S = 0.65$ – $0.75$  (Table 1). The inclusion of  $(M_0S)^5$  and  $(M_0S)^6$  terms reduces the error to 1.6–4.1%.

## 10. High $z$ Expansion

For peaks or high densities the expansion (for small  $y$ ) will not converge, and results are subject to computational precision errors. The value of the  $z$  expansion [see Eq. (21)] is small as can be seen from  $f = 1/(\ln y)$  itself (Fig. 7): Near  $y = 1$  it is similar to  $1/(y \ln y)$ , and the integral of  $f$  is dominated by the first terms. Below  $y \approx 0.25$  the two functions show no similarity, and  $f$  tends to zero with the convex shape of an increasingly negative slope as  $y = 0$  is approached. The area between  $y = 0$  and  $y_1$  of this curve is bounded by the line from the origin to  $(y_1, 1/(\ln y_1))$  and by the extension of the slope at this point to the  $y$  axis. The upper bound is  $y_1/(2 \ln y_1)$ , and the lower bound is  $[y_1/(\ln y_1)][1 - 1/(2 \ln y_1)]$ . These may be compared with the convergence of the  $z$  expansions above for various values of  $y_1$ , since the expansion will differ from this area by a constant ( $-0.5772$ ), which is derivable to arbitrary accuracy by observation of the limiting values as  $y_1 \rightarrow 0$ . They may also be compared with the integral of  $g = 1/(y \ln y)$ , which

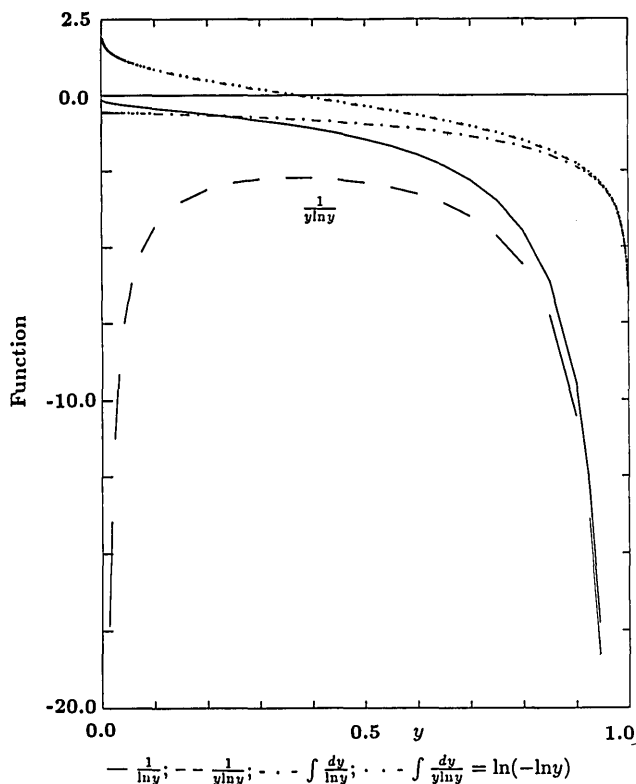


Fig. 7. Comparison of  $1/(\ln y)$ ,  $1/(y \ln y)$  and their integrals against  $y = (0, 1)$ .

corresponds to the first term in Eq. (24) and the first term of the remaining expansions (Table 2).

The  $z$  expansion may be given either by the convergence of the expansion (for low  $z$ ) or by the limit at zero plus either area estimate (for high  $z$ ). Background and fogging should follow the low- $z$  expansion, with the lower- $z$  limit increasing with exposure and density.  $z_{\min}$  may sweep through the transition region, for high energies, or may remain in the low region. This explains the variety of possible toe shapes and the length of the toe region on  $D - \ln I$  curves as a function of emulsion ( $\sigma$  and  $M_0S$ ) and the energy of the radiation (through the scaling factor and  $z_{\min}$ ). Higher-energy  $x$  rays show extended toe regions.<sup>16</sup> Table 3 and Fig. 8 show that the scale

factor  $[\sin \theta / (\mu' 2.30\bar{d}) = 3.42$  for  $E = 7$ -keV radiation] yields strong exposure of the grains ( $D \approx 3.0$ ) while  $z$  lies below 1.5. For  $E = 1.7$  keV, conversely, any exposure yielding a density greater than unity must lie in the linear regime. Essentially no density arises from values of  $z < 0.01$ .

Truncation of the  $(M_0S)^n$  expansion (for  $n > 4$ ) underestimates densities for strong exposures ( $\sigma\beta I > 1.4$ ) and high packing densities ( $M_0S > 0.55$ ) by a few percent. Early truncation of the  $z$  expansion adds significant (5%) oscillations to linear and transition regions of the  $D - \ln I$  curve for all energies. The limiting value replacing the expansion at high  $z$  may range from the exact value at the cutoff  $z$  to the  $y = 0$  limit. For truncation after  $z^4$  terms, the cutoff arises around  $z = 2.2$ , and the limit may vary from  $-0.6145$  to  $-0.5772$ . This can yield oscillating final errors in  $D$  of 30%. We may obtain increased precision by including  $z^5$  and  $z^6$  terms. The limit may then be taken as the mean of the range from  $-0.5772$  to  $-0.5990$  at a  $z = 2.6$  cutoff [with the errors from (2) and (3) in Table 3] or more accurately as  $-0.5772 + \Delta$ , where  $\Delta$  is the mean of the upper and lower bounds of Table 2 [with the errors indicated in group (4) of Table 3]. The largest errors are given in the fourth and seventh columns of Table 3, reaching 1% from the  $z$  expansion and 4% from neglect of  $(M_0S)^n$  terms,  $n > 6$ . This is appropriate over the full range of densities and energies for  $M_0S \leq 0.75$  and is much more efficient than nonanalytic integration. Additional terms may become significant for  $M_0S > 0.75$ , but this prescription is much more accurate than earlier forms, with errors of only 10–20% for  $M_0S \approx 0.95$ .

## 11. Basic Model Equations

The use of  $d_0$  to allow for the first layers<sup>6</sup> is of a similar form to Eq. (19b) and is an empirical approximation to the correct summation. Using Eqs. (19a), (20), (24), and the results in Table 3 suggests two forms for the photographic density–exposure relation [Eqs. (25a) and (25b)]. A third form [Eq. (25c)] may be derived by use of  $z_m' = \sigma\beta I$  in Eq. (25a), modeling a rough surface (where the front surface of the first grain defines the front of the emulsion, which is varied locally by  $\bar{d}$ ) compared with the planar emul-

Table 2. Area Estimates for  $\int \frac{dy}{\ln y} = \ln z - z + \frac{z^2}{4} - \frac{z^3}{18} + \dots < 0$

Values of $y$	0.50	0.25	0.05	0.01	0.001	$10^{-5}$
$\frac{1}{\ln y}$	-1.443	-0.7215	-0.3338	-0.2172	-0.1448	-0.0869
Values of $z = -\ln y$	0.693	1.386	2.996	4.605	6.908	11.51
First term ( $\ln z$ )	-0.3665	+0.3266	+1.0972	+1.5272	+1.9327	+2.4432
Terms in $z$ required <sup>a</sup>	5–7	7–9	11–14	14–18	20–24	32–36
Expansion limit ( $\int^z$ )	-0.9559	-0.6959	-0.5903	-0.5791	-0.5774	-0.5772
Area ( $\int_0^z$ ) upper bound	-0.3608	-0.0902	$-8.35 \times 10^{-3}$	$-1.09 \times 10^{-3}$	$-7.24 \times 10^{-5}$	$-4.35 \times 10^{-7}$
Area ( $\int_0^z$ ) lower bound	-0.2010 <sup>b</sup>	-0.1153	$-1.39 \times 10^{-2}$	$-1.94 \times 10^{-3}$	$-1.34 \times 10^{-4}$	$-8.31 \times 10^{-7}$

<sup>a</sup>For estimated 1–0.01% precision of the expansion.

<sup>b</sup>This bound is inappropriate here.

Table 3. Integrals to Convergence Over Ranges of  $z$  of  $\int \frac{\ln[1 - M_0S(1 - y)]dy}{y \ln y}$

	0.990	0.905	0.50	0.25	0.05	0.01	0.001
$y_{\max}$	0.990	0.905	0.50	0.25	0.05	0.01	0.001
$y_{\min}$	0.905	0.500	0.25	0.05	0.01	0.001	$10^{-5}$
$z_{\max}$	0.100	0.693	1.386	2.996	4.605	6.908	11.51
$z_{\min}$	0.010	0.100	0.693	1.386	2.996	4.605	6.908
Integrals: 1st = $\int \frac{dy}{y \ln y} = [\ln z]$ ; 2nd = $\int \frac{dy}{\ln y} = [\ln z - z + \dots]$ ; $\dots$ [Eq. (24)]							
First	2.2958	1.9379	0.6931	0.7706	0.4300	0.4055	0.5108
Second	2.2084	1.4459	0.2600	0.1055	0.0113	0.0017	0.0001
Integrals <sup>a</sup>	5	5	3	2	2	1	1
Terms required <sup>a</sup>	3-4	4-6	6-8	8-12 <sup>b</sup>	12-16 <sup>b</sup>	16-22 <sup>b</sup>	22-34 <sup>b</sup>
(1) Total: $\int \frac{\ln[1 - M_0S(1 - y)]dy}{y \ln y}$ [expression in parentheses in Eq. (24)]							
( $M_0S = 0.75$ )	0.0669	0.4208	0.4358	0.7663	0.5152	0.5037	0.6390
( $M_0S = 0.65$ )	0.0578	0.3576	0.3607	0.6196	0.4119	0.4018	0.5095
( $M_0S = 0.55$ )	0.0488	0.2970	0.2921	0.4909	0.3228	0.3142	0.3982
(2) Estimated correction for $M_0S_n$ terms, $n < 4$ (estimated error)							
	(%)	(%)	(%)	(%)	(%)	(%)	(%)
( $M_0S = 0.75$ )	+0.002	+0.13	+1.41	+5.3	+8.6	+9.6	+9.7
( $M_0S = 0.65$ )	+0.001	+0.07	+0.76	+2.8	+4.4	+4.9	+5.0
( $M_0S = 0.55$ )	+0.001	+0.03	+0.38	+1.3	+2.1	+2.3	+2.3
(3) Effect of truncation after $z^6$ with limit = -0.5881 for $z > 2.6$							
	(%)	(%)	(%)	(%)	(%)	(%)	(%)
( $M_0S = 0.75$ )	+0.002	-0.2	+2.5	-3.0	+4.4	+0.7	+0.04
( $M_0S = 0.65$ )	+0.001	-0.2	+1.9	-2.4	+4.1	+0.6	+0.04
( $M_0S = 0.55$ )	+0.001	-0.1	+1.4	-2.0	+3.8	+0.6	+0.04
(4) Effect of truncation after $z^6$ , $(M_0S)^6$ terms, versus exact result							
	(%)	(%)	(%)	(%)	(%)	(%)	(%)
( $M_0S = 0.75$ )	-0.00	-0.8	+1.5	-2.9	-2.8	-4.0	-4.2
( $M_0S = 0.65$ )	-0.00	-0.5	+1.0	-1.6	-0.7	-1.4	-1.6
( $M_0S = 0.55$ )	-0.00	-0.3	+0.6	-0.9	+0.1	-0.4	-0.5

<sup>a</sup>Required for estimated 0.1% precision of the limits.  
<sup>b</sup>Higher integrals require many terms and reach precision limits.

sion surface of Eq. (25a).

$$D = \frac{-1}{2.30} \ln\{1 - M_0S[1 - \exp(-z_m')]\} + \frac{\sin \theta}{2.30\bar{d}\mu'} H(z_{\min}, z_{\max}, M_0S),$$

$$z_{\max} = \sigma\beta I \exp(-\mu' \bar{d} / \sin \theta),$$

$$z_{\min} = \sigma\beta I \exp[-\mu'(T - \bar{d}) / \sin \theta],$$

$$z_m' = \begin{cases} \sigma\beta I \frac{\sin \theta}{\mu_0 \bar{d}} [1 - \exp(-\mu_0 \bar{d} / \sin \theta)] & \sigma\beta I < 1 \\ \sigma\beta I \exp[-\mu_0 \bar{d} / (2 \sin \theta)] & \sigma\beta I > 1 \end{cases} \quad (25c)$$

(25a)

$$D = \left( \frac{\sin \theta}{\mu'} + d_0 \right) \frac{1}{2.30\bar{d}} H(z_{\min}, z_{\max}, M_0S),$$

$$z_{\max} = \sigma\beta I, \quad z_{\min} = \sigma\beta I \exp[-\mu'(T - \bar{d}) / \sin \theta], \quad (25b)$$

$H(z_{\min}, z_{\max}, M_0S)$

$$= \left\{ \left[ M_0S + \frac{(M_0S)^2}{2} + \dots + \frac{(M_0S)^6}{6} \right] [\ln z]_{z_{\min}}^{z_{\max}} - \frac{M_0S[1 - (M_0S)^6]}{1 - M_0S} [G(z)]_{z_{\min}}^{z_{\max}} + \left[ \frac{(M_0S)^2}{2} + (M_0S)^3 + \dots + \frac{5(M_0S)^6}{2} \right] [G(z)]_{z_{\min}}^{z_{\max}} - \left[ \frac{(M_0S)^3}{3} + (M_0S)^4 + 2(M_0S)^5 + \frac{10}{3}(M_0S)^6 \right] \times [G(z)]_{z_{\min}}^{z_{\max}} + \left[ \frac{(M_0S)^4}{4} + (M_0S)^5 + 2.5(M_0S)^6 \right] [G(z)]_{z_{\min}}^{z_{\max}} - \left[ \frac{(M_0S)^5}{5} + (M_0S)^6 \right] [G(z)]_{z_{\min}}^{z_{\max}} + \frac{(M_0S)^6}{6} [G(z)]_{z_{\min}}^{z_{\max}} \right\} \quad (25d)$$

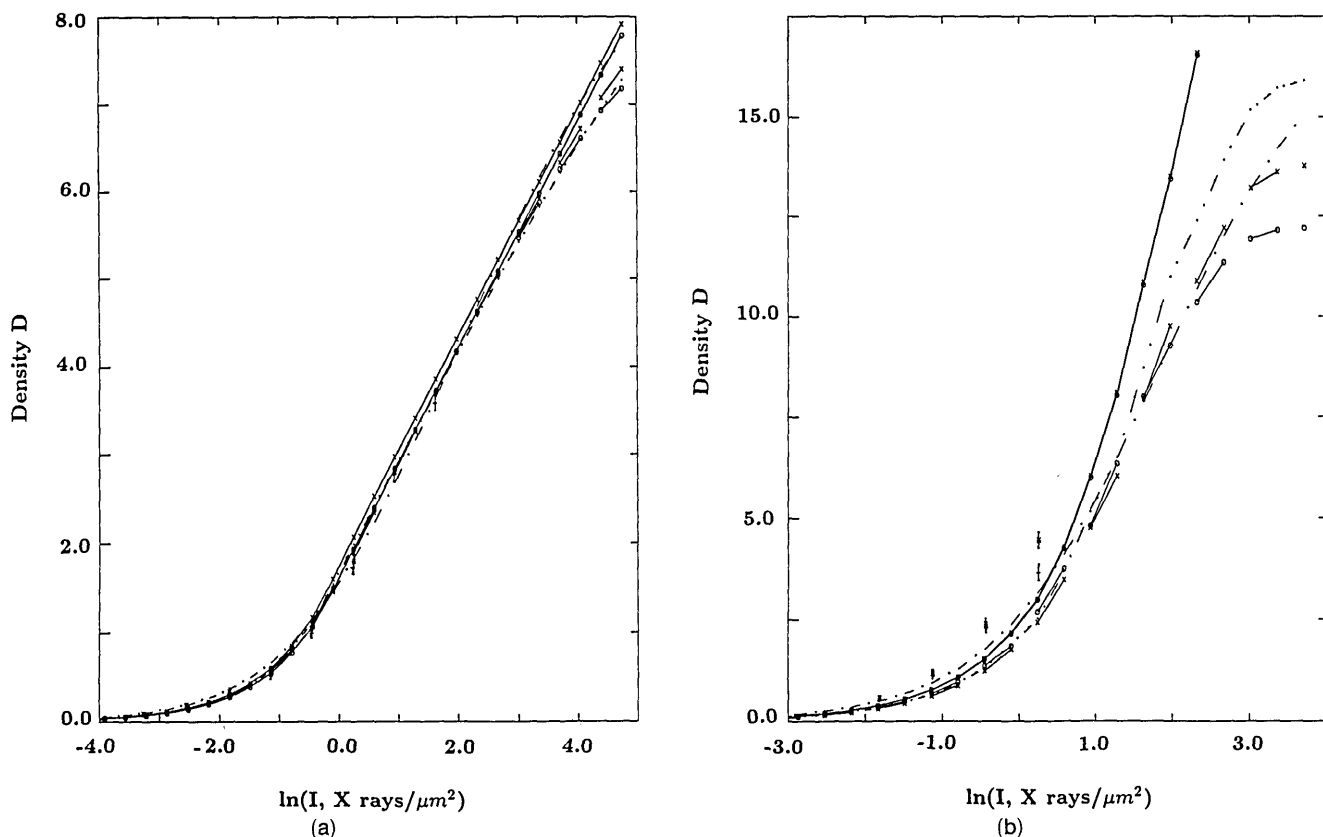


Fig. 8.  $D$ - $\ln I$  relations for DEF emulsion and (a) 1.74 keV and (b) 6.93 keV (+) radiation with models from Table 4, as mentioned in Fig. 6 and the text. Corrected (+) and uncorrected (\*) data are compared with modeling. The lower energy reaches the linear  $D$ - $\ln I$  regime above  $D \approx 1$ , which ends above  $D = 6$ -10, depending on the model. Conversely higher-energy x rays follow this regime for  $D \approx 3$ -22 or  $D = 4$ -10.

$$G(z) = \begin{cases} \ln z - z + \frac{z^2}{4} - \dots + \frac{z^6}{6!6} & z \leq 2.2, \\ -0.5772 + \frac{y}{2z} \left( \frac{1}{2z} - 1.5 \right), & \\ y = \exp(-z) & z > 2.2. \end{cases} \quad (25e)$$

The truncation of integrals follows naturally when upper and lower limits reach  $-0.5772$ . We may evaluate integrals crossing the transition region by summing contributions from low-, mid-, and high- $z$  regions as above. (Table 3 gives examples for  $M_0S = 0.55$ - $0.75$ .) Alternatively, the number of integrals to be evaluated at a given precision may be given by  $z_{\text{lim}}$ , so that the evaluation of low- $z$  limits ( $z \leq 0.1$ ) involves all five integrals but requires only  $\ln z - z$  terms of each. Such constraints could be implemented, but this prescription [Eqs. (25)] is short and finite. The evaluation for  $z < 0.001$  reveals the imprecision of the  $M_0S$  coefficients, but the integral is negligible for  $z_{\text{min}} < 0.001$ .

## 12. Homogeneous Attenuation Coefficients, Scattering, and Photoelectrons

The parameter  $\beta$  involves  $\mu_0$ ,  $\mu_1$ , and  $\mu_w$ . We interpolated them from available tables versus energy from 5-20 eV to 20 keV,<sup>18-21</sup> given the elemental composi-

tion of the materials and assuming that atomic photoabsorption dominates over reflection and scattering processes. The tables are generally consistent and in agreement with experiment at the 2% level for high energies, with larger uncertainties for UV wavelengths and absorption edges. Valence orbitals, molecular absorption bands, and excitons have dominant effects on absorption coefficients below 5-10 eV, where atomic absorption tables become inadequate.

Elastic scattering by AgBr grains and gelatin develops surface grains rather than deep layers but has a small effect compared with the visible region where the phase is coherent and nearly constant over the grain diameter and scattering amplitudes sum. The coefficients per atom increase with energy: as low as CuK $\alpha$  (8.05 keV), scattering coefficients for AgBr and gelatin are, respectively, 2% and 7% of the photoabsorption coefficients; thus they are important secondary effects. The angular distributions of scattered radiation are complex, but a simple approximation is adequate here: Scattering reduces the intensity from the incident beam and directs it on average along the same depth in the emulsion. For medium energies or broad sources this may then expose other grains at this depth of the emulsion or may be absorbed by the gelatin.

Inelastic scattering can lead to the multiple expo-

sure of grains per x ray. We could accommodate this by altering  $\mu_1$  to include  $\sigma_{\text{inelastic}}$  (but not  $\sigma_{\text{elastic}}$ ) in  $\beta$  while including both in  $\mu'$ . The scattered radiation may then develop additional grains. Below energies of 20 keV inelastic scattering contributes <0.5% to density.

Attenuation coefficients at higher energies requires an allowance for elastic scattering. Previous transmission measurements at 8.05 keV overestimated the grain fraction by neglecting scattering. One may estimate scattering followed by grain absorption by replacing  $[1 - \exp(-\mu_1 d')]$  in  $\beta$  [Eq. (1)] with

$$\begin{aligned} & \{1 - \exp[-(\mu_1 + \sigma_{\text{inc}}^1) d']\} \\ & + \{1 - \exp[-(\mu_1 + \sigma_{\text{inc}}^1) d' / 2]\} \sigma_{\text{scat}}^1 d' \\ & + \exp[-(\mu_1 + \sigma_{\text{inc}}^1) d' / 2] (\sigma_{\text{scat}}^1 + \sigma_{\text{inc}}^1) \\ & \times d' \frac{(\%v/v)\mu_1}{(\%v/v)\mu_1 + (1 - \%v/v)\mu_0} \\ & + (\sigma_{\text{scat}}^0 + \sigma_{\text{inc}}^0) d' \frac{(1 - \%v/v)\mu_1}{(\%v/v)\mu_1 + (1 - \%v/v)\mu_0}, \quad (26) \end{aligned}$$

which represents terms for absorption in the grain before or after scattering and single scattering by grain ( $\sigma^1$ ) or gelatin ( $\sigma^0$ ) prior to absorption by the given grain. For DEF at 8 keV, the first term dominates and is 1.2% larger than the value neglecting scattering, the second and third contribute 2.2%, and the fourth has a relative magnitude of 0.1%. The total correction is similar to  $\{1 - \exp[-(\mu_1 + \sigma_{\text{inc}}^1 + \sigma_{\text{scat}}^1) d']\}$ , which increases the first term by 1.7%. Expressions should be reconsidered for  $E > 20$  keV but are adequate in the current range. Window and supercoat scattering coefficients may also be included.

Photoelectron development of multiple grains becomes significant when the mean photoelectron range in AgBr exceeds  $\bar{d}/3$  and is capable of initiating two secondary sites when it exceeds  $\bar{d}$ . For 10-keV photoelectrons the range may be estimated to be 0.67  $\mu\text{m}$  in AgBr grains or 1.6  $\mu\text{m}$  in gelatin,<sup>22</sup> compared with the estimated DEF emulsion  $\bar{d} \approx 1.6 \mu\text{m}$ . Narrow-angle scattering can lead to the exposure of a grain immediately below the initial location, which reduces the effect slightly. This rises as  $E^x$ , where  $x = 1.9$ . X rays of 8 keV produce photoelectrons primarily by interaction with Ag and Br atoms, with energies of 4.7 and 6.5 keV, respectively. Absorption coefficients of Ag and Br give the relative fraction of each. The resulting ranges may then be used with the estimates of nearest-neighbor distances to scale  $\beta$  by  $(1 + \delta_{\text{photo-e}})$ , which at 8 keV is of the order of 1.025. Photoelectrons from gelatin yield a smaller correction.

### 13. Emulsion Structure

The composition of gelatin appears in the derivation of  $\mu_0$  (for the supercoat),  $\mu_0$  (for the first effective layer), and  $\mu'$  (the heterogeneous absorption coefficient). That for the grains appears in  $\mu_1$  (for the

exposure of a grain) and in  $\mu'$ . A common assumption of gelatin as  $\text{C}_3\text{H}_{16}\text{O}_5\text{N}_2$  with  $\rho = 1.4\text{g cc}^{-1}$  is also used here; it represents the dominant proteinaceous component (glycine, proline, hydroxyproline, alanine) while other organic matter and a sulfurous component in particular are neglected. The latter constituents are minor.

After the inclusion of iodides in the grain, with adsorbed KBr, gelatin particles, and sensitizing agents (sulfurous or organic), the constitution of the grain is  $[\text{AgBr}(\text{AgI})_w]_x(\text{KBr})_y(\text{gel})_z(\text{sen})_a$ ,  $a, w \ll 1$ , and  $y, z \ll x$ . The iodide forms an intrinsic part of the crystal lattice, and other constituents are largely adsorbed onto the surface.<sup>23</sup> Emulsions such as 101-07 lack a gelatin coating but still have adsorbed salts and gelatin particles. Here  $z$  can be considered part of the gelatin matrix or a small supercoat thickness,  $w$  and  $y$  have similar absorption coefficients to AgBr, and exposure generally requires absorption within the  $x$  component rather than the  $y, z$ , or  $a$  components, which recovers the AgBr formula for grains.

Variations from the mean emulsion thickness  $T$  occur, especially at the edges and emulsion holes or where cracks develop.<sup>17</sup> This shifts the background level or puts a glitch in the observed spectra, but it is otherwise insignificant. The initial normal distribution of grain sizes followed by growth proportional to size (as during ripening) yields a model of the distribution of AgBr grain sizes in the emulsion.<sup>16</sup> For the emulsions considered herein, the grains are nearly spherical (from the electron microscopy micrographs).

### 14. Heterogeneous Absorption Coefficients

The equations used above and elsewhere use mean values of  $d$  or  $\exp(-\mu d / \sin \theta)$  etc., where  $d$  may refer to the mean diameter of a grain, the mean path length through a grain, or the mean distance between grains. These values should be averaged over the grain distribution and circular cross section. The average over the grain size distribution is a small effect, dependent on unknowns, and neglected here.

The homogeneous linear absorption coefficient of the emulsion of evenly distributed AgBr and gelatin  $\bar{\mu}$  diverges at low energies from the heterogeneous coefficient  $\mu'$ , allowing for the clustering of grains of mean path length  $d'$ . The grains are common assumed to be aligned cubes with no variation in either  $d$  or the mean path length.<sup>3,6,10,11</sup> This gives the coverage per layer for cubes as  $\%v/v$ , the mean path length through each grain as  $d' = \bar{d}$ , and a summation over the grain encounters of a photon leads to an average transmission factor  $\tau$  through a distance  $x$  of

$$\begin{aligned} \tau &= \sum_{n=0}^{x/\bar{d}} z_n \tau_n = \exp(-\mu' x) \\ &= \exp(-\mu_0 x) (1 - \%v/v) [1 - \exp[-(\mu_1 - \mu_0) \bar{d}]]^{x/\bar{d}} \quad (27) \end{aligned}$$

and hence<sup>3,6</sup>

$$\mu' = \mu_0 - \frac{1}{\bar{d}} \ln(1 - (\%v/v)[1 - \exp[-(\mu_1 - \mu_0)\bar{d}]]) \quad (28a)$$

This corresponds to a reduction of  $\bar{\mu}$  by an energy-dependent factor of 30% for DEF and 1–2 keV or an error from use of the homogeneous coefficients of 2–3 in linearized intensity. Grains approximate spheres, not cubes, which have a mean path length per grain of  $d' = (2\bar{d})/3$  and a mean coverage for a monolayer of depth  $\bar{d}$  of  $M_0\sigma_g \approx (3/2)(\%v/v)$ . Summing over path-length steps of  $d'$ , assuming that  $\mu_0 < \mu_1$ , yields

$$\mu' = \mu_0 - \frac{3}{2\bar{d}} \ln\left(1 - \frac{2}{3} M_0\sigma_g \left\{1 - \exp\left[-(\mu_1 - \mu_0)\frac{2}{3}\bar{d}\right]\right\}\right) \quad (28b)$$

This further modifies the absorption coefficient for 1–4-keV energies. Above 10 keV,  $\bar{\mu}$  and Eq. (28b) are equivalent. For photons incident at an angle, this becomes

$$\mu' = \begin{cases} \mu_0 - \frac{3}{2\bar{d} \sin \theta} \ln(1 - (\%v/v)\sin \theta \\ \times \{1 - \exp[-(\mu_1 - \mu_0)\frac{2}{3}\bar{d}]\}) & \mu_0 \leq \mu_1 \\ \mu_1 - \frac{3}{2\bar{d} \sin \theta} \ln(1 - [1 - (\%v/v)\sin \theta] \\ \times \{1 - \exp[(\mu_1 - \mu_0)\frac{2}{3}\bar{d}]\}) & \mu_0 > \mu_1 \end{cases} \quad (28c)$$

However, the implicit assumption of random and uncorrelated grain positions in each layer is false, and the assumption of a mean value is increasingly inaccurate for grains in the first few half-layers of the emulsion. These models are illustrated in Fig. 9, and a comparison of values is given in Fig. 10.

Spherical grains in the upper half of the first monolayer of the heterogeneous emulsion cannot overlap one another; thus the coverage of AgBr resulting from this depth is

$$M_1\sigma_g = G_{\text{tot}}\sigma_g/A_d = \frac{\%v/v}{V_0} \frac{\bar{d}}{2} \sigma_g \approx 0.3 \text{ (DEF emulsion).}$$

Grains in the next half-layer are negatively correlated with this layer (they fill up the holes), and the absorption coefficient for these particles is therefore typically  $\mu_0$  over the path length  $\bar{d}/2$  and neither  $\mu_1$  nor  $\mu'$ . The sum over layers [Eq. (3a)] neglects  $\mu_0\bar{d}/2$ , while the corresponding integral [Eq. (4)] assumes that  $\mu_0 = \mu'$  for these particles. The correction factor  $d_0$  in Eqs. (5) and (25b) and the use of summations of the form of Eqs. (3a), (10a), (12), (19a), and (19b) are empirical or partial corrections for this correlation. The modifications of Eqs. (10b), (25a),

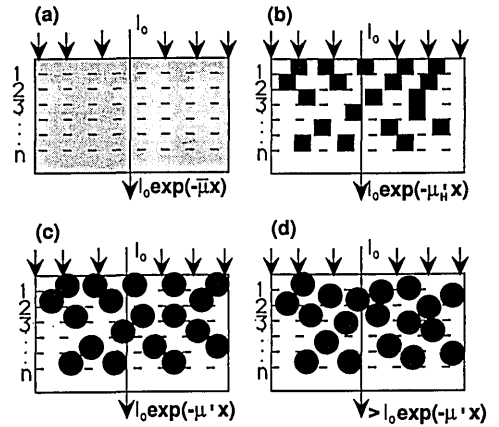


Fig. 9. Models for absorption calculations: (a) Homogeneous model yielding  $\bar{\mu}$ . (b) Heterogeneous model from Ref. 8 where stacked, aligned cubes in layers of thickness  $d$  [Eq. (28a)] are assumed. (c) Heterogeneous model where stacked spheres (diameter  $\bar{d}$ ) in layers of  $(2\bar{d} \sin \theta)/3$  thickness are assumed, the correct coverage per path length is used, and  $\mu_0 > \mu_1$  [Eq. (28c)] is allowed for. (d) Effect of variation in grain depth on the first two layers.

and (25c) help to avoid neglect of the  $\mu_0$  or  $\mu'$  variation within each layer.

### 15. Effect of Spherical Grains on Equations

Equations (1) and (18) implicitly assume that a mean path length through a grain may be used rather than

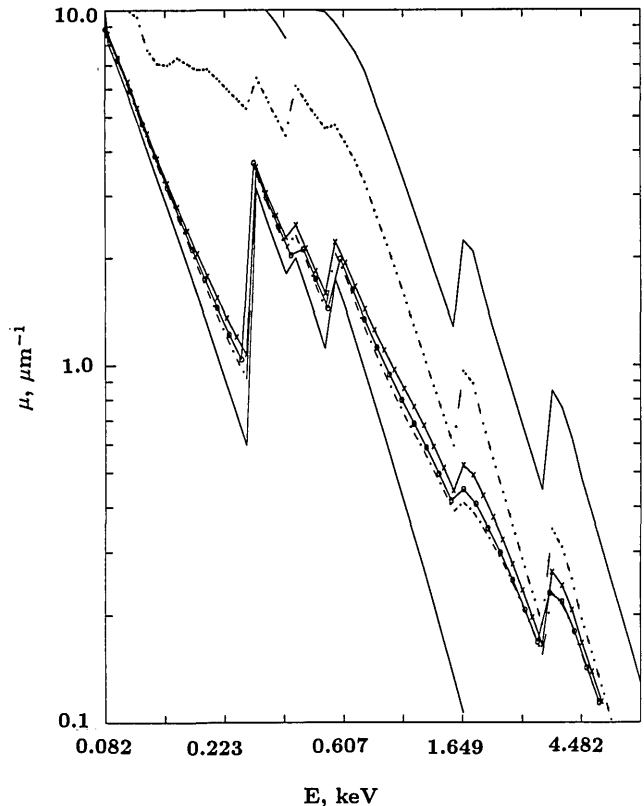


Fig. 10. Attenuation coefficients for DEF emulsion parameters. Solid curves represent  $\mu_0$  and  $\mu_1$  for gelatin and AgBr grains with  $\cdots$  for  $\bar{\mu}$ ,  $\cdots$  for  $\mu'$  of Eq. (28a), and  $\cdots$  and  $\cdots$  for Eq. (28c) at normal incidence and  $0.1R$ , respectively.

the path-length distribution. For high energies or low absorption, this equates to the geometric mean  $(2\bar{d})/3$ . The photon path length through the emulsion prior to the grain  $x$  varies with the impact parameter from the grain center. Smooth and rough models of Eqs. (25a) and (25c) may be compared in the distribution of ranges of  $x$  prior to the grain surface.

For a given impact parameter  $0 < r < (\bar{d}/2)$  at a mean grain,  $P(r)dr = (8rdr)/\bar{d}^2$  in the physical range of possible  $x$  values, varying from  $x(r=0) = 0 \rightarrow T - \bar{d}$  (normal incidence) to  $x[r = (\bar{d}/2)] = (\bar{d}/2) \rightarrow T - (\bar{d}/2)$ . The former extreme has  $d'(r=0) = \bar{d}$  with  $d'[r = (\bar{d}/2)] = 0$ . The generalization for  $\theta = (\pi/2)$  and  $x$  is

$$x(r) = \frac{\bar{d} - d'}{2} \rightarrow T - \frac{\bar{d} + d'}{2},$$

$$d'(r) = \bar{d} \left[ 1 - \left( \frac{2r}{\bar{d}} \right)^2 \right]^{1/2}, \quad P(r) = \frac{8r}{\bar{d}^2}. \quad (29)$$

For arbitrary  $0 < \theta < (\pi/2)$  there are two lower limits of  $x(r)$  from the branches  $[\bar{d}/(2 \sin \theta)](1 - \cos \theta) > x(r) > 0$  and  $0 < x(r) < [\bar{d}/(2 \sin \theta)](1 + \cos \theta)$ . These yield the lower limits  $x(r) = [\bar{d}/(2 \sin \theta)] - d'/2 \pm r \cot \theta$ . The difference between the upper and lower limits of  $x$  is always  $T - \bar{d}$  (hence we have the integration and summation limits in the above equations). This reveals an error in Eqs. (4)–(7) caused by the assumption of an upper limit  $x_{\max} = T$  instead of  $T - \bar{d}$ . The error is significant near saturation.

Rough and smooth surface models have identical values of  $d'(r)$  and  $P(r)$ , and the physical locations within the emulsion are invariant, but the rough model has air or vacuum between the grains in the first half-layer. In the rough case the initial value of  $x(r)$  (the depth in the emulsion prior to the grain) is therefore zero. This is more sensitive to low-energy  $x$  rays than the smooth model. For a given photon the effective mean value of  $d'$  is not simply  $(2\bar{d})/3$  but includes the effect of attenuation through the grain path and, for the smooth model, the additional path through the emulsion for  $r > 0$ . The latter involves  $\mu_0$  for the first layer or  $\sim \mu'$  for subsequent monolayers.

The models replace  $1 - \exp(-\mu_1 d')$  in Eq. (1) *et seq.* with

$$J = \int_{r=0}^{\bar{d}/2} \frac{8r}{\bar{d}^2} K [1 - \exp(-\mu_1 d'(r))] dr, \quad (30a)$$

$$K\left(\theta = \frac{\pi}{2}\right) = \begin{cases} 1 & \text{rough surface model,} \\ \exp[-\mu_0(\bar{d} - d')/2], & \text{smooth model,} \\ & \text{first monolayer,} \\ \exp[-\mu'(\bar{d} - d')/2], & \text{smooth model,} \\ & \text{later monolayers.} \end{cases} \quad (30b)$$

This yields solutions

$$\frac{2}{A^2} [A - 1 + \exp(-A)] + \frac{2}{(\mu_1 \bar{d} - A)^2}$$

$$\times [(\mu_1 \bar{d} - A) \exp(-\mu_1 \bar{d}) + \exp(-\mu_1 \bar{d}) - \exp(-A)] \quad \text{smooth model:}$$

$$A = \frac{\mu_0 \bar{d}}{2}, \quad \text{first monolayer,}$$

$$A = \frac{\mu' \bar{d}}{2}, \quad \text{subsequent layers,}$$

$$1 + \left[ \frac{2 \exp(-\mu_1 \bar{d})}{\mu_1 \bar{d}} \right] + \frac{2}{(\mu_1 \bar{d})^2} [\exp(-\mu_1 \bar{d}) - 1], \quad \text{rough model.} \quad (30c)$$

The two models agree in the  $A \rightarrow 0$  limit and reduce to the geometric for  $\mu_1 \bar{d} \rightarrow 0$ . For general angles the problem is more complex, and the coverage of the *rough* model must be defined carefully. The first half of the first mean grain is assumed to be not covered by gelatin, but the deeper fraction of the grain is assumed to be bound to the gelatin matrix. Then

$$K(\theta) = \begin{cases} \frac{\exp[-\mu_0[\bar{d}/(2 \sin \theta) - d'/2 + r \cot \theta]] + \exp[-\mu_0[\bar{d}/(2 \sin \theta) - d'/2 - r \cot \theta]]}{2}, & \text{smooth model, first layer,} \\ \frac{\exp[-\mu'[\bar{d}/(2 \sin \theta) - d'/2 + r \cot \theta]] + \exp[-\mu'[\bar{d}/(2 \sin \theta) - d'/2 - r \cot \theta]]}{2}, & \text{later monolayers,} \\ 1, & \text{rough surface, } r \leq \frac{\bar{d}}{2} \sin \theta, \\ 0.5\{1 + \exp[-\mu'(r \cot \theta - d'/2)]\}, & r \geq \frac{\bar{d}}{2} \sin \theta, \text{ later monolayers.} \end{cases} \quad (30d)$$

These equations appear to bear no analytic solution but (1) the component remaining at  $\theta = \pi/2$  may be isolated and solved, leading to precise solutions for  $\theta \approx \pi/2$ , (2) for low absorption the  $\mu_0$  or  $\mu'$  exponentials may be expanded and the result integrated, and (3) for high absorption the exponential coefficients may be transformed to a linear function of the integrating variable, and the function multiplying the exponential may be expanded in a rapidly convergent power series for most angles.

Unfortunately (3) fails at  $r = (\bar{d}/2) \sin \theta$ , the peak of the function. Regions crossing the singularity must be integrated differently by, e.g., expanding circular functions in the exponential. This generates an error function (to second order) and an approximate solution. The prescription works reasonably well for all angles and energies but is less efficient than direct numerical integration. Rough and smooth models reduce to the results above for normal incidence or high energies and give the extremes of expected emulsion behavior.

An *intermediate* model is also indicated in Fig. 11. The latter is computationally simple and lies between rough and smooth model extremes for grazing angles above  $0.5^R$ . The prescriptions for rough and smooth models are identical to results obtained numerically for normal incidence and are accurate to a few percent for most angles. The poorest agreement (10% discrepancy) is obtained for the smooth model at  $45^\circ$  and low energies, where the truncation of terms and the effects of the singularity are most significant. Use of a geometric average  $d' = (2\bar{d})/3$  leads to good agreement for energies above 0.25 keV at normal incidence [Fig. 11(a)] or above 3.0 keV at near-grazing incidence, but it is not valid below these energies. An improved approximation for the high-energy regime of type (2) is given for angles  $1.0^R$ ,  $(\pi^R/4)$ , and  $0.1^R$ , illustrating that the prescription above converts to this approximation (and back again) at different energies and absorption coefficients, as a function of the angle.

The rough and smooth models show a complex dependence of  $J$  on energy and angle. Conversely the value assumed previously<sup>6-8</sup> is unity below 1 keV, only approaches the current models for energies above 20 keV, and has no dependence on angle [Figs. 11(a) and 11(d)]. The closest agreement to this earlier factor is given by the rough model at normal incidence. At normal incidence and in the energy range from 0.93 to 8.05 keV for which DEF data are available, the earlier coefficient should be reduced by 0-30%.

## 16. Comparison of Formulas Over the Characteristic Curve

The limiting behavior of Eqs. (25a) and (25b) and Section 11 may be compared with Eq. (6), where  $a$  and  $b$  are empirical fitting coefficients in addition to  $d_0$  and where the inadequacy of the function and the correlation of these parameters distort  $d$  and  $T$ .

The linear region for very low exposures follows naturally for Eq. (25b) (permitting  $z < 0.01$ ); note

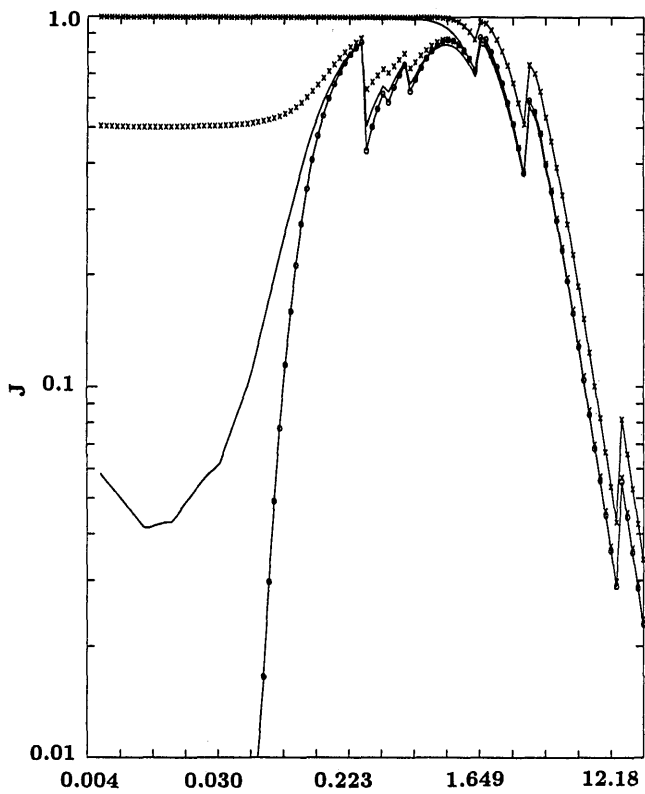
that the coefficients of  $\ln y$  cancel [a result of the  $(1-y)^n$  expansion], and higher powers of  $z$  are negligible; thus the remaining term is proportional to  $\Delta z = \sigma\beta I\{1 - \exp[\mu'(T - \bar{d})/\sin \theta]\}$ . This yields [for Eqs. (6), (25b), and (25a)]

$$\begin{aligned}
 D(6) &\rightarrow \frac{a}{\alpha} b\beta I[1 - \exp(-\mu'T/\sin \theta)], \\
 D(25b) &\rightarrow \left(\frac{\sin \theta}{\mu'} + d_0\right) \frac{M_0 S}{2.30\bar{d}} \\
 &\quad \times \sigma\beta I\{1 - \exp[-\mu'(T - \bar{d})/\sin \theta]\}, \\
 D(25a) &\rightarrow \left(\frac{M_0 S \sin \theta}{2.30\bar{d}}\right) \sigma\beta I\left(\frac{1}{\mu_0} [1 - \exp(-\mu_0\bar{d}/\sin \theta)] \right. \\
 &\quad \left. + \frac{1}{\mu'} \{\exp(-\mu'\bar{d}/\sin \theta) \right. \\
 &\quad \left. - \exp[-\mu'(T - \bar{d})/\sin \theta]\} \right). \quad (31)
 \end{aligned}$$

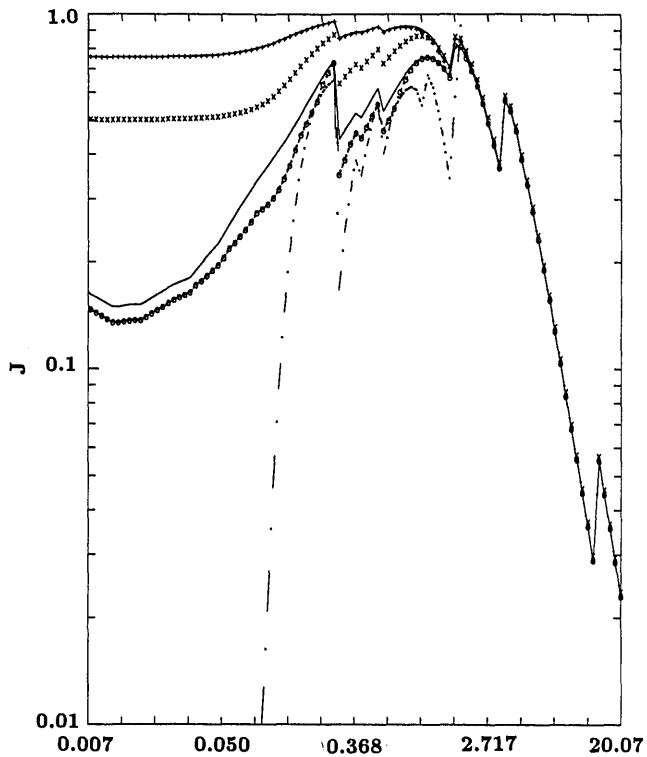
The discrepancy between Eqs. (25a) and (25b) indicates the expected energy dependence of  $d_0$  and the limitations of these formulas over the first two layers. Ideally  $\mu$  should vary smoothly from  $\mu_0$  to  $\mu'$  as a function of depth. Equation (25a) should approximate this behavior, and  $d_0$  may be fitted over a suitable energy range to bring Eqs. (25a) and (25b) into agreement. Identification of  $b \approx \sigma$  and  $a \approx (M_0 S/2.30\bar{d})$  leads to agreement between Eqs. (25b) and (6) and is implied in Henke *et al.*'s model.<sup>6</sup> However, the coefficients obtained in empirical fits by Henke *et al.* for DEF emulsion yield  $b = 1.69 \mu\text{m}^2$  versus  $\sigma \approx (\pi/4)\bar{d}^2 \approx 2.01 \mu\text{m}^2$  and  $a = 0.68 \mu\text{m}^{-1}$  versus  $(M_0\sigma/2.30\bar{d}) \approx 0.163 \mu\text{m}^{-1}$ .

Part of this discrepancy was due to neglect of  $d_0$  in the application of the model and to the correlation between  $a$  and  $b$ . Different heterogeneous coefficients, integrating thicknesses of  $T$  instead of  $T - \bar{d}$ , neglect of scattering and photoelectron contributions, and use of  $d' = \bar{d}$  in  $\beta$  all contribute to this discrepancy.  $I_p$  derived through Eqs. (6) and (7) should give grain distributions and densities through Eqs. (3) and (9)-(12) in agreement with the observed density. The result, for low densities that fit Eq. (6) and agree with experiment, is low by a factor of 5. This indicates the nonphysical nature of these parameters. At the saturation limit the equations become

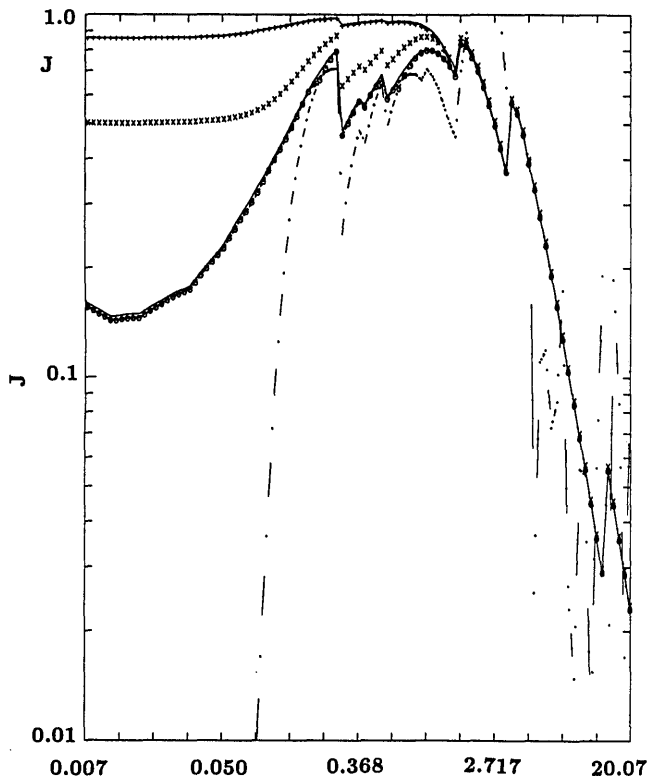
$$\begin{aligned}
 D(6) &\rightarrow \frac{a \mu' T}{\alpha \sin \theta}, \\
 D(25a) &\rightarrow \left[ M_0 S + \frac{(M_0 S)^2}{2} + \dots + \frac{(M_0 S)^6}{6} \right] \left( \frac{T}{\bar{d}} - 1 \right) \\
 &\quad \left/ 2.30 \approx \frac{-\ln(1 - M_0 S)}{2.30} \left( \frac{T}{\bar{d}} - 1 \right), \right. \\
 D(25b) &\rightarrow \frac{-\ln(1 - M_0 S)}{2.30} \left( \frac{T}{\bar{d}} - 1 \right) \left( 1 + \frac{d_0 \mu'}{\sin \theta} \right). \quad (32)
 \end{aligned}$$



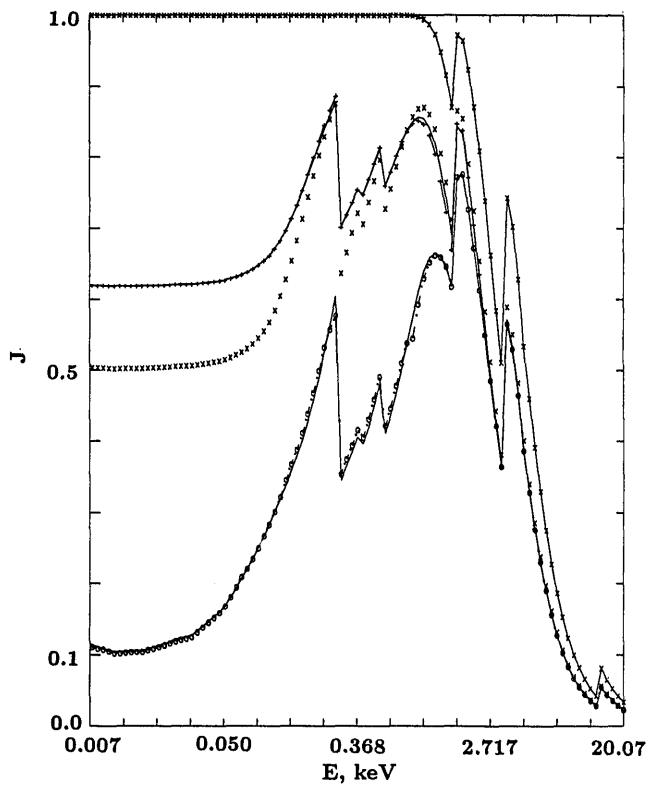
(a)



(c)



(b)



(d)

Fig. 11. (continued.)

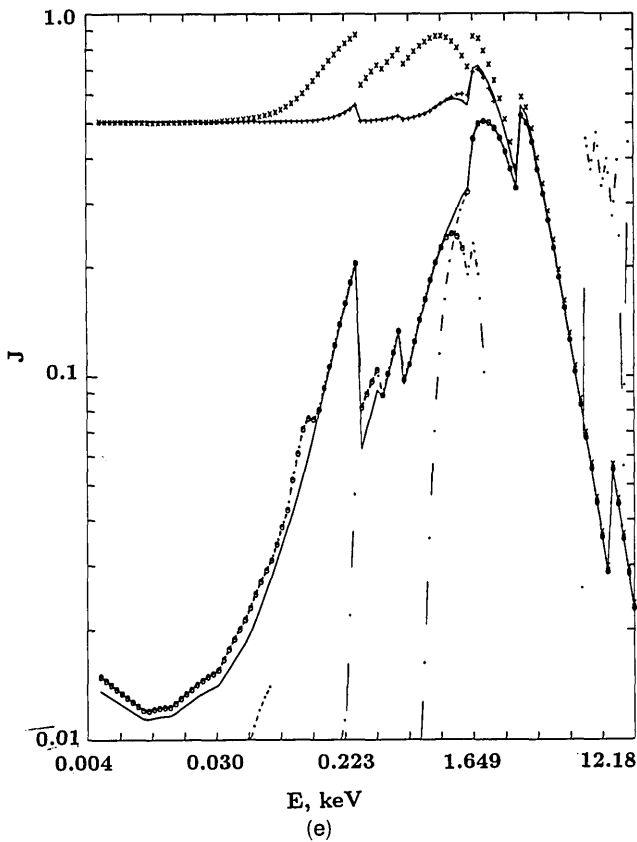


Fig. 11.  $J$  coefficients for the mean value of  $\exp(-\mu x) [1 - \exp(-\mu_1 d')]$ , Section 15, averaged over a spherical grain for rough and smooth emulsion surfaces (upper and lower solid curves) compared with a simple intermediate model ( $\times$ ) and the prescription of Ref. 8 ( $-\times-$ ). They are presented for (a) normal incidence [ $\theta = (\pi/2)R$ ], (b)  $1.0^R$ , (c)  $(\pi/4)^R$ , (d)  $0.5^R$ , and (e)  $0.1^R$  to show the sharp variation of exact and approximate forms with the incident angle. In (a) the geometric average ( $-\circ-$ ) is shown to give a large error for energies of  $< 0.2$  keV and is worse than but similar to the low-absorption approximation of the smooth coefficient of (b)–(e) ( $\cdot-\cdot$ ). The prescription given in the text for an analytic estimation of the coefficient is given in (b)–(e) for rough and smooth cases ( $+\text{---}+$ ,  $\circ-\circ$ ). For normal incidence they are exact, while the greatest error is obtained for a smooth model approximation at  $(\pi/4)^R$ .

Given the earlier identification of  $a$  and  $b$ , Eq. (6) shows discrepancy by a factor of

$$\frac{-M_0 S T}{(T - \bar{d}) \ln(1 - M_0 S)}$$

( $\approx 0.75$  for  $M_0 S = 0.6$ ,  $\approx 0.36$  for  $M_0 S = 0.95$ ),

which indicates a low-coverage approximation. Equation (25a) shows no energy or angular dependence at this limit, while other expressions include factors of  $(d_0 \mu') / (\sin \theta)$ . This indicates the form  $d_0$  requires in order to yield a sensible model and suggests a limitation of validity of Eqs. (6) and (25b) in the high-density, low-energy regimes.

The linear regime of the  $D - \ln I$  curve follows from 6 when  $\exp(\mu' T / \sin \theta) \gg b \beta I \gg 1$ . The range of  $I$  showing this behavior is clearly energy and angle dependent, corresponding to  $z_{\max} > 3$ ,  $1 \gg z_{\min}$ . For high energies or thin emulsions this criterion may never be valid, and the transition regions cover the range of the curve. Where it is valid, Eqs. (25a) and (25b) become identical except for  $d_0$ :

$$D(6) = \frac{a}{\alpha} [\ln(b \beta I) - b \beta I \exp(-\mu' T / \sin \theta)]$$

$$= \frac{a}{\alpha} F = \left( \frac{\sin \theta}{\mu'} + d_0 \right) \frac{1}{2.30 \bar{d}} M_0 S F,$$

$$D(25b) \rightarrow \left( \frac{\sin \theta}{\mu'} + d_0 \right) \frac{1}{2.30 \bar{d}} L,$$

$$D(25a) \rightarrow \frac{\sin \theta}{2.30 \mu' \bar{d}} L,$$

$$L = [\ln(\sigma \beta I) + 0.5772] \times \left[ M_0 S + \frac{(M_0 S)^2}{2} + \dots + \frac{(M_0 S)^6}{6} \right] - M_0 S \sigma \beta I \exp[-\mu'(T - \bar{d}) / \sin \theta]. \quad (33)$$

The main difference lies here in the low-coverage approximation of Eq. (6) and the omission of the 0.5772 offset. Since  $a$  is fixed by the low-exposure limit and the saturation region is neglected, the limiting density will be erroneous. Over the linear region,  $b$  may adjust its value to accommodate for the omission of 0.5772 and other terms. This behavior is observed in these papers.<sup>6-8</sup> In other papers<sup>3,10</sup>  $d'$  and  $\bar{d}$  are similarly confused, absorption in various regimes is neglected, and serious low and high  $z$  approximations are made. The former also treats  $d_0$  as a constant but alters the exponential in the denominator of Eqs. (6) so that the saturation limit is better preserved.

At high densities Eqs. (6) and (7) may be expected to fail, while at low densities they can be accurate. The low-coverage approximation and reduced heterogeneous attenuation coefficient are compensated for in part by the increased effective thickness and the empirical 10–20% reduction in  $b$  to fit the lower part of the linear region and the toe.

## 17. Comparison to Experiment for DEF Emulsion

Comparison of these models with data involves correction for diffuse versus specular density. For DEF emulsion the most comprehensive studies have been done by Henke *et al.*<sup>8</sup> and Rockett *et al.*<sup>11</sup> The former converted the data of the latter to specular density ( $0.1 \times 0.1$  numerical aperture) using

$$D_{0.1} = 1.9D_d - 0.35D_d^2 + 0.092D_d^3 \quad (34a)$$

fitted over the region  $0.1 < D_d < 2.5$ . The range of validity appears to be  $0.1 < D_d < 1.9$ , at which point the slope  $D_{0.1}/D_d = 1.567$  and begins to rise. The relations found in all other emulsions show a slow but continuous decline of this ratio with increasing  $D_d$  (often exponentially toward unity).<sup>3,7,11</sup> Justification for this is given by Brown *et al.*,<sup>3</sup> who present a curve that is analogous to data for DEF, extended to  $D_d = 4.5$ , and calculated for Kodak No-Screen film, assuming an acceptance angle of  $5.2^\circ$ . Below  $D_d = 1.7$  this is consistent with the formula and data of Henke *et al.*; above  $D_d = 1.2$  it may be characterized by  $D_{0.1} \approx 1.8D_d - 0.08D_d^2$ . This slope and intercept depend on emulsion characteristics and the model.

Equation (34a) may be contrasted with measurements in Ref. 11 over  $0.25 < D_d < 3.0$ , which yielded  $D_{0.1} \approx 2.18D_d - 0.25D_d^2$  (0.93-keV radiation) or  $D_{0.1} \approx 2.13D_d - 0.17D_d^2$  (6.93-keV radiation). These relations are inadequate below  $D_d = 0.6$  or above  $D_d = 4.0$ , where ratios below unity would be predicted. A synthesis of these data is here given by the use of Eq. (34a) below  $D_d = 1.9$  with

$$D_{0.1} = (1.567 - A)D_d + AD_d \exp[-k(D_d - 1.9)], \\ \pm 0.03(D_d - 1.9)D_d, \quad D_d > 1.9, \\ A = 0.567, \quad k = 0.4626, \quad (34b)$$

which leads to a physical ratio for high densities and the extrapolation error above this range.  $A = 0.367$  and  $k = 0.8491$  would fit the data equally well in the range  $1.9 < D_d < 3.0$  and yield a physical limit in the  $D_d > 4.0$  region; hence it provides an error estimate. Errors below this range are estimated from the size of plotted points and the consistency of data.

An additional set of data for CuK $\alpha$  energies is provided by Ref. 9 and converted as given in Ref. 8 to specular values. There are difficulties in both the conversion factor above and in the initial measurement of density and intensity for all sets of data, especially above densities of 3–4, as discussed by Rockett *et al.*,<sup>11</sup> Phillips and Phillips,<sup>9</sup> and (in our case) Section 3 (see also Chap. 4 of Ref. 13 and Sec. 4 of Ref. 24). Since the models assume that background densities are negligible, there is the possibility of an incorrect ratio of  $D/I$  in this region below densities of 0.1. Equations (34a) and (34b) should be applied relative to unexposed film rather than a background level, following which the converted background may also be subtracted. In Ref. 8 this procedure is not consistently followed, and it is adjusted therein to give a linear  $D/I$  relation at low energy.

This shift is avoided in the current treatment, but if applied it would increase densities from Ref. 11 for 0.93 keV by 0.03 and for 1.74 keV by 0.017 and reduce those for 4.51 keV by up to 0.02. The densities in Ref. 8 for 8.05 keV may be reduced by up to 0.03, those for 0.93 keV lack sufficiently low-density data, and the remainder is in agreement at the 0.001 level. Discrepancies may imply uncertainty in low-density measurements at this level.

Henke *et al.*<sup>8</sup> fitted Eq. (6) to three energies for which independent duplicate measurements were obtained. For the 0.93-keV energy the data obtained above  $D = 2.0$  were neglected, as were data below  $D = 0.25$ . Data above  $D = 2.0$  were neglected for  $E = 1.49$  keV, which relates to the uncertainties and errors discussed above. These data are included in the current modeling. The extension to double-sided emulsions is analogous to Eq. (7) of Ref. 8. The data therein for 8.05 keV appear to conflict with the model of Henke *et al.* in the same paper, especially at low densities, and are omitted in the current modeling, while the data of Rockett *et al.* for 1.74 keV appear to agree with the implementation of Eq. (6) and are included. The data of Ref. 11 for mixed 4.51 + 4.93 keV energies of Henke *et al.*, and for 6.93 keV, are rejected by Ref. 8, are not in agreement with the modeling of Henke *et al.*, and are also omitted from current modeling.

Given the six data sets of four energies, the model and coefficients of Eq. (6) yield a reduced  $\chi^2$  of 3.3. Typically the model is high around the  $D = 0.5$ – $1.0$  region and low for high densities. The optimized coefficients for current equations yield reduced  $\chi^2$  values of 2.4 for the smooth model [Eq. (25a)],  $\sim 5.8$  for the rough model [Eq. (25c)], and 2.5 and 2.2 for rough and smooth models using  $d_0$  and Eq. (25b). On this basis the emulsion is probably smooth, and models in this paper appear to be superior to those used earlier. The parameters in Table 4 show curious behavior and question the physical significance of the final result.  $C_f$  and  $S_f$  relate to the effective cross section per grain divided by the geometric cross section  $\{\sigma/[(\pi/4)\bar{d}^2]\}$  and the increase in cross section on development  $\{S/[(\pi/4)\bar{d}^2]\}$ ; the values listed for Ref. 8 use  $b/[(\pi/4)\bar{d}^2]$  and  $(2.30\bar{d}a)/(M_0\sigma_g)$  for comparison, neglecting other effects.

The best fit to the smooth model yields an unacceptably large emulsion thickness with relatively large ratios  $C_f$  and  $S_f$ . Reducing the thickness to a plausible value still provides a good fit to the data and is inadequate only for the 8.05-keV data. The rear emulsion gives no contribution for energies below 3.6 keV, as is true for lower layers of the first emulsion. The failure for 8.05 keV may be due to inadequate allowance for the rear emulsion or other effects but is probably a consequence of the neglect of correlation of attenuation with depth, particularly for deeper layers. Use of  $d_0$  distorts the physical significance of variables, particularly  $S_f$ . Final  $\chi_r^2$  values are dependent on estimated data uncertainties. Fits involve highly correlated parameters, so relatively small er-

Table 4. Optimized Coefficients for DEF Parameters Compared with Experimental Determinations and Previous Values

Model	Parameter								
	$\%v/v$	$t_0$ ( $\mu\text{m}$ )	$T$ ( $\mu\text{m}$ )	$t_b$ ( $\mu\text{m}$ )	$d$ ( $\mu\text{m}$ )	$d_0$ ( $\mu\text{m}$ )	$C_f$	$S_f$	$\chi^2$
Ref. 8, Eq. (6)	0.40	1.0	13.0	185.0	1.6	0.0	0.84	4.17	3.3
Ref. 11	0.40	1.3	13.0	177.6	1.6	—	1.51	2.00	—
Experiment	0.38	1.1	$14.2 - t_0$	177.6	1.6	—	> 1	1-2	—
	$\pm 0.03$	$\pm 0.7$	$\pm 0.7$	$\pm 7.4$	$\pm 0.3$	—	?	?	—
Smooth, Eq. (25a)	0.386	1.68	24.0	(185)	1.50	—	2.30	2.00	2.4
Smooth, Eq. (25a)	0.384	1.78	14.2	(185)	1.54	—	2.36	1.99	3.0
Smooth, Eq. (25b)	0.41	2.0	13.5	(185)	1.69	0.59	2.26	2.25	2.2
Rough, Eq. (25b)	0.41	2.0	13.5	(185)	1.56	0.38	2.35	2.35	2.5

rors can lead to significant uncertainty for any given parameter. The base thickness has been assumed to be 185  $\mu\text{m}$ , but a lower value of such as 177.6  $\mu\text{m}$  would also be possible subject to the base attenuation at 8.05 keV being 0.85 (all references agree on this result).

If all developed clusters within a layer covered different areas, an increase in area of  $S_f = 2.0$  would yield a total coverage of  $M_0S = M_0\sigma_g S_f = 1.2$  at saturation for DEF. Instead developed clusters overlap, and  $M_0S \approx 0.94$ , corresponding to an effective  $S_f \approx 1.6$ . This latter value has been applied in the above, but also for low coverages, where the effective  $S_f$  should be 2.0. The use of a constant effective  $S_f$ , independent of depth in the emulsion and density, will increase predicted saturation densities and decrease low-density values in some regimes. These effects are not obvious in Figs. 6, 8, and 12, but parameter values may be distorted.

The data correspond to the first transition region at most energies. Plots of  $D-I$  indicate that the linear low-density regime ends at densities of 0.6–2, dependent on energy. The data set omitted for 8.05 keV is presented in Fig. 6 and is compatible with most models. The data set for 4.51 keV is incompatible with any model, even after the diffuse/specular conversion correction. The correction improves agreement of the 6.93-keV data with fitting [Fig. 8(b)], especially compared with Henke *et al.*'s model. The inclusion of all data sets yields a reduced  $\chi^2$  for models of  $\sim 8.9$ , suggesting that the reasons for exclusion are valid.

The fitted models diverge in the linear  $D - \ln I$  region and bear little similarity at saturation. Unfortunately this corresponds to densities of 12–28, which are not measurable under standard densitometry conditions (see Fig. 2). Extrapolation from fitted models to lower and higher energies leads to the rapid divergence of predicted results. This problem, with that of extrapolation to higher densities, limits the usefulness of current model simulations. For this purpose it is interesting to model 101 emulsion sensitivity.

**18. Comparison with Experiment for 101 Emulsion**

The data for 101 have been extracted from Henke *et al.*<sup>6,7</sup> and Burton *et al.*<sup>12</sup> Although the densitometry is similar, the data sets relate to 101-07 and 101-01,

respectively. The main difference is the nature of the base composition, which is of no significance since 101 is a single-emulsion film. The sensitivity variation between batches is quoted as “better than a factor of 2” as is agreement with other calibrations: This is enough to question both experimental results and the use of these data sets together, especially for  $D < 0.3$  results. Fogging and exposure to air reduce sensitivity, especially below 5–10 eV.

Despite these caveats the combination of parts of these data sets from widely differing energies provides sensitive measurement of emulsion parameters and the applicability of extrapolation involving standard models. In Ref. 7 nine energies between 109 and 2293 eV were used. Only those for 277 and 524.9 eV were presented in full and are used here as representative of the higher-energy range. In Ref. 12 are results for 12 energies between 4.4 and 16.9 eV: Those for 5.25, 9.51, 10.33, 11.62, and 16.87 eV are used as representative of results above 5.0 eV.

It is perhaps impressive that current models are able to fit such a range of densities and energies at all. In Ref. 6 the higher-energy data were fitted to a three-parameter thin emulsion model. In the fitted regions, discrepancies were observed up to 30% or 0.2 in density, with data lying consistently above the fitting curve for  $D < 0.8$ . This model cannot be extrapolated to other energies or densities with these parameters, as indicated by the reduced  $\chi^2$  in Table 5 and Fig. 13. For these data use of a model with no emulsion would yield a much improved  $\chi_r^2 = 159$ . The thick emulsion formula [Eq. (6)] enables  $\chi_r^2 = 28$  to be obtained after inclusion of the empirical parameter  $d_0$ ; even so the form of the relation is invalid below 200 eV. Conversely models in this paper cover the full range of energies and densities with  $\chi_r^2 = 13$ .

The uncertainties in the data account for part of this result. They are estimated from grain errors and quoted uncertainties but neglect calibration errors at low densities. In particular the low densities at 5.25 and 11.62 eV are not linear with intensity. At 5.25 eV this could be due to reciprocity law failure (several photons being required per grain for exposure), but this is less likely for 11.62 eV, particularly as intermediate energies have no such nonlinearity. If this is due to background subtraction error, the densities should be increased in each case by 0.10, doubling or tripling the value at the minimum data

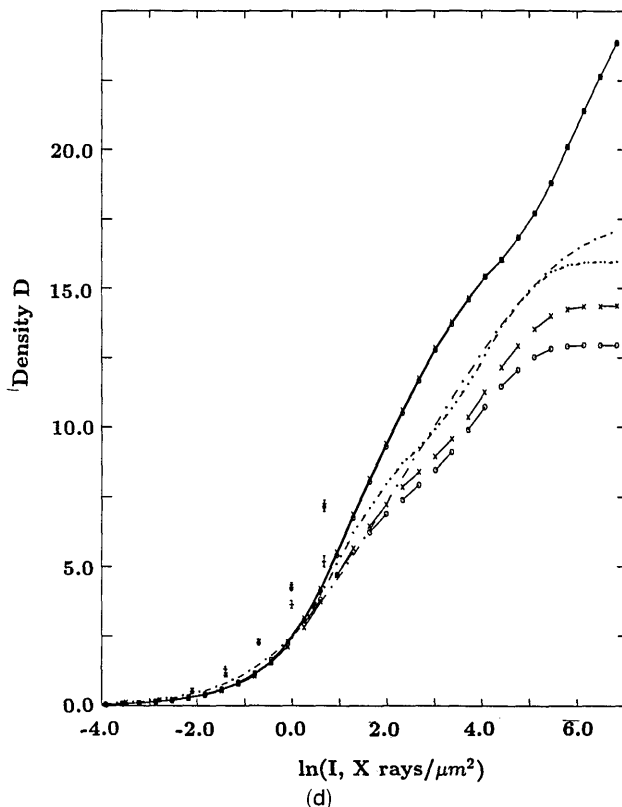
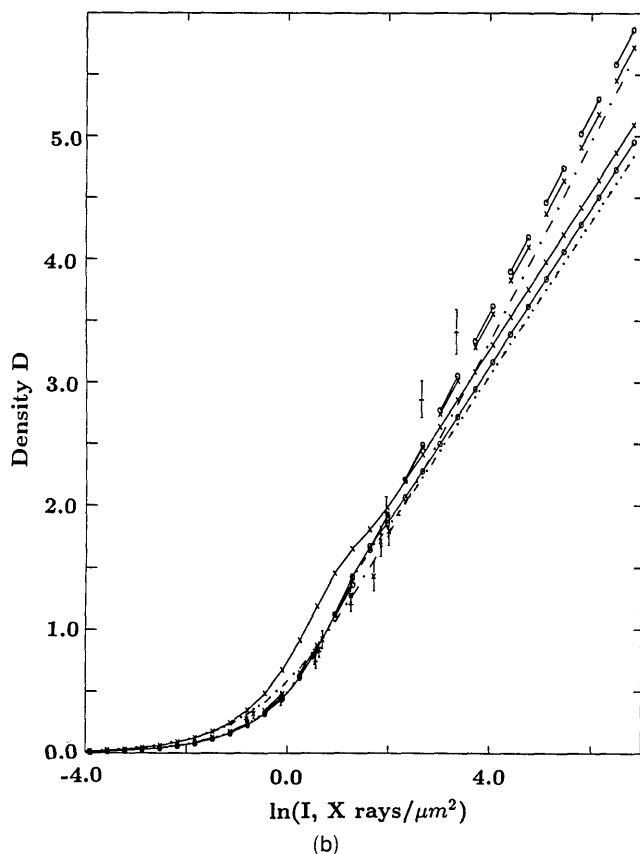
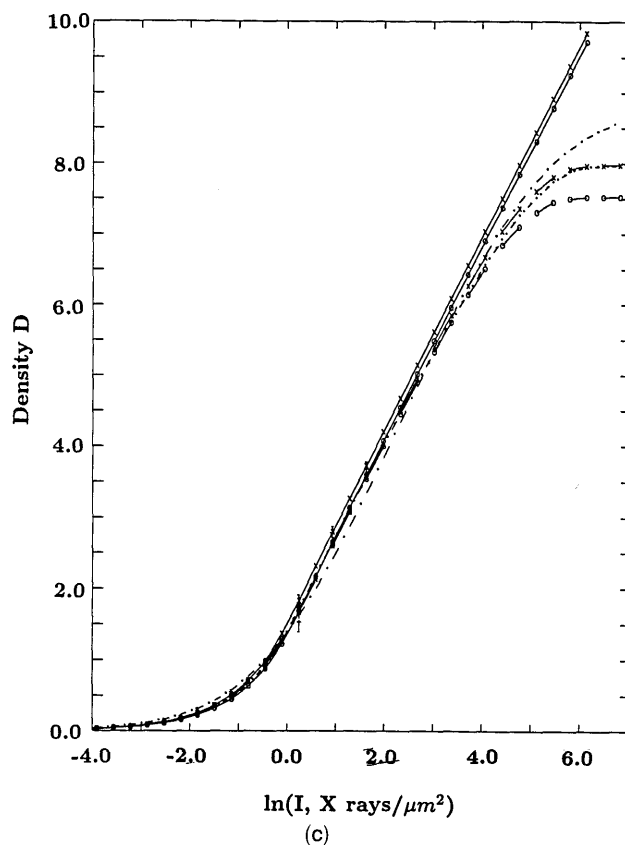
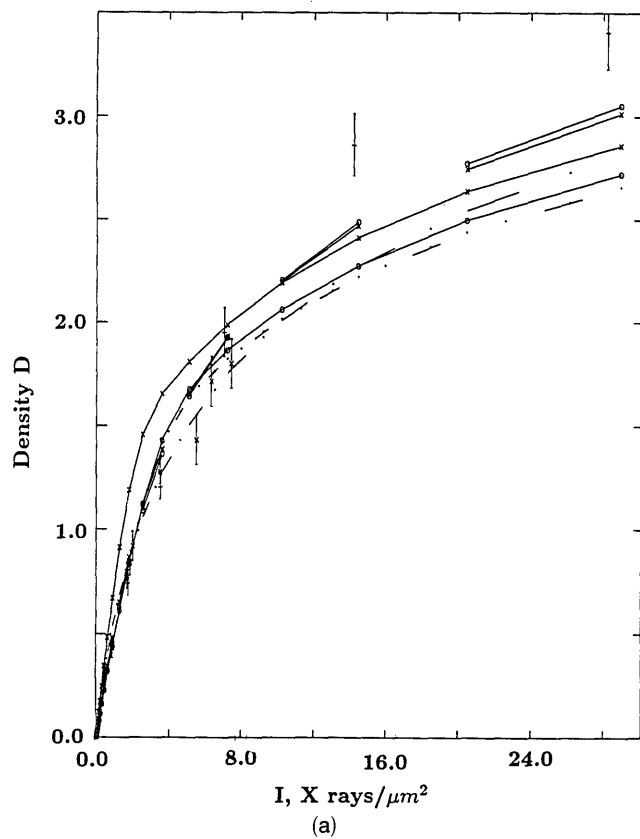


Fig. 12.  $D$ - $\ln I$  relations for DEF emulsion and (a), (b) 0.93-keV, (c) 1.49-keV, and (d) 4.51 + 4.93-keV radiation with models from Table 4, as mentioned in Fig. 6 caption and the text. Corrected ( $\times$ ) and uncorrected ( $*$ ) data are compared with modeling. The lower energy follows the linear  $D$ - $I$  relation below  $D \approx 0.5$ - $0.9$  (a) and reaches the linear  $D$ - $\ln I$  regime above  $D \approx 1.4$ - $1.8$ , which ends above  $D \approx 6$ . The regimes are poorly defined for 4.51 keV, and experimental conditions are such that poor agreement with corrected or uncorrected data is expected.

Table 5. Optimized Coefficients for 101 Parameters Compared with Experimental Determinations and Previous Values<sup>a</sup>

Model <sup>a</sup>	Parameter								
	% <i>v/v</i>	<i>t</i> <sub>0</sub> (μm)	<i>T</i> (μm)	<i>d</i> (μm)	<i>d</i> <sub>0</sub> (μm)	<i>C<sub>f</sub></i>	<i>S<sub>f</sub></i>	$\chi_r^{2b}$	$\chi_r^{2c}$
Ref. 8, Eq. (6)	0.74	0.0	0.6	0.6	0.0	1.06	6.69	60	58
Ref. 8	0.73	0.0	0.6	0.65	0.035	0.95	6.47	28	23
Experiment	0.74	0.0	1–2	0.85	—	> 1	1–2	—	—
	±0.1	±0.1	±1.0	±0.25	—	?	?	—	—
Rough, Eq. (25c)	0.74	0.0495	Mono	0.7155	—	1.47	1.53	13.2	10.0
Rough, Eq. (25c)	0.74	0.0524	Mono	0.850	—	1.50	1.535	—	7.4
Rough, Eq. (25c)	0.74	0.052	Mono	0.915	—	1.27	1.535	—	7.4
Rough, Eq. (25b)	0.74	0.050	1.87	1.20	0.64	1.31	1.40	—	5.5

<sup>a</sup>Thin-emulsion model<sup>6,7</sup>:  $a = 1.957, b = 0.3128 \mu\text{m}^2, T = 2.0 \mu\text{m}, \chi_r^2 = 33340, b 23000$ .

<sup>b</sup>Using all data and initial errors.

<sup>c</sup>Corrected as discussed in text.

point of each set, with uncertainties of a similar magnitude. Absorption coefficients of 5.25 eV have significant uncertainty, extrapolated from 8 to 10 eV with potentially large molecular contributions. This data set was therefore removed from the subsequent fitting procedure, and uncertainties in the 11.62-eV data set were increased so that they overlap with a linear low-intensity response.

The smooth model [Eq. (25a)] is unable to fit the data with  $\chi_r^2 < 100$ . This is physically a consequence of the absence of gelatin covering the surface and a relative absence of a supercoat. DEF emulsion contains this coating and agrees with this model as a consequence; it is claimed that 101 emulsion lacks this coating, and hence it should not agree with the smooth emulsion formulation. At higher energies (277–525 eV) this is less important, and the rough and smooth model predictions converge, but at lower energies the model is invalid [Figs. 13(d) and 13(e)].

The rough emulsion model [Eq. (25c)] agrees with the data ( $\chi_r^2 = 7.4$ ) and minimizes toward a monolayer model. It has been stated that 101 is a monolayer, but the thin-emulsion model deduced  $T = 2.0 \mu\text{m}$ , whereas  $d = 0.7 \rightarrow 1.0 \mu\text{m}$ , implying a two- to three-layer emulsion. Iteration from  $T = 2 \mu\text{m} \approx 3\bar{d}$  leads to  $T/\bar{d} < 2$ , at which point the integral of Eq. (25c) vanishes, leaving the simple result

$$D = -\ln[1 - a_1[1 - \exp(-b_1I)]], \quad (35)$$

where  $a_1$  is the effective coverage of the fully developed emulsion and  $b_1$  contains the only energy dependence. If the emulsion is thicker than a monolayer and less than a bilayer, the effective coverage will increase but other effects on absorption coefficients and densities will be minor. The effective coverage is fitted to be  $a_1 = 0.978$  and is a function of %*v/v* and  $S_f$ , which is in good agreement with expected values.

The best fit is provided by the rough emulsion model with Eq. (25b) and the (large) empirical  $d_0$  parameter. This shows agreement with all data above 6 eV and minimizes toward a 1.5-layer model. The parameters are in reasonable agreement with experimental estimates and with results in Eq. (25c) and are relatively undistorted, as opposed to other

models.<sup>6–8</sup> Rough model predictions diverge from the data and from each other above  $D = 1.8$  [Figs. 13(c) and 13(e)], but the low-energy high-density data lie between the two predictions. This divergence corresponds to an alternative treatment of the initial layers, neither perfect, but both useful, of similar value, providing an error estimate for this region. The discrepancy may be expected from the high coverage after development.

The models require a supercoat thickness of 50 nm, which may be interpreted as a real supercoat, a coating around each grain, or a model with some smooth emulsion character. The coating around each grain is required for stability, and the real emulsion is probably not quite so rough as the model assumption.

### 19. Observations on the Dependence of Response on the Angle of Incidence

Although the literature demonstrates good agreement with the integral model presented here, it all relates to normal-incidence work, and there is a dearth of tabulated measurements and comparisons for other angles. There should be a future investigation of this, which may also help to support the angular dependence presented here as opposed to that of Eqs. (1)–(6). The dependence is summarized in the explicit occurrence of  $\theta$  in Eqs. (25) [versus Eqs. (5) and (6)] together with the implicit dependence of  $\mu'$  contained in Eq. (28c) [versus Eq. (28a)] and the dependence of  $z$  on  $\mu', \theta$ , and  $\beta$  as indicated in Eqs. (25) versus Eq. (1). Finally the dependence of  $\beta$  on angle is not simply given following Eq. (3b) but requires the modifications discussed in Section 15 and represented by Eqs. 30.

These changes have been explained pictorially as a function of energy and explicitly for  $\mu'$  and  $J, \beta$  in Figs. 10 and 11, respectively. It can be seen that the angle  $\theta = 0.1^R$  versus  $(\pi/2)^R$  leads to changes in  $\mu'$  by from negligible values to 15% or so, depending on energy, and to changes by up to 20% from the earlier value [Eq. (28a)].

The earlier value for  $J$  or  $\beta$  is erroneous by 50%, 25%, and 15% at 12, 2, and 1 keV energies, respec-

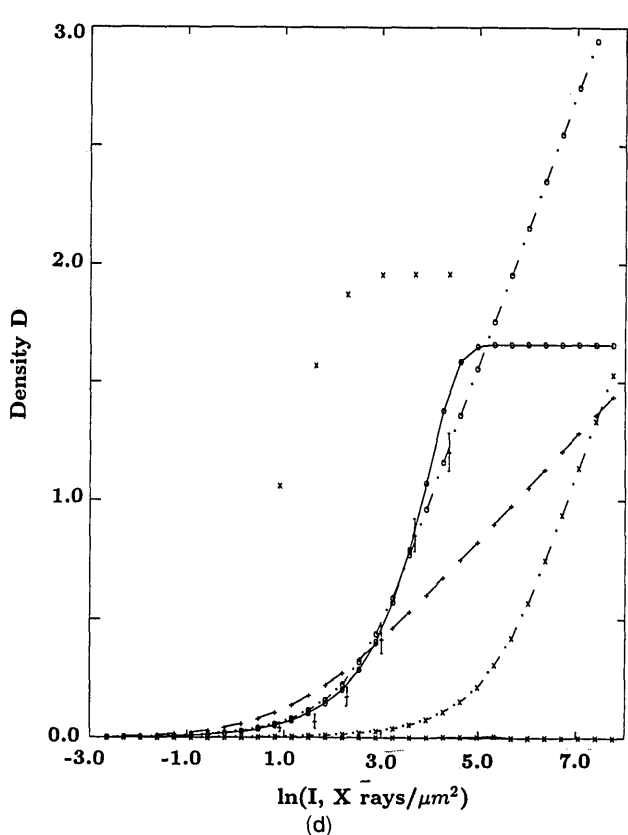
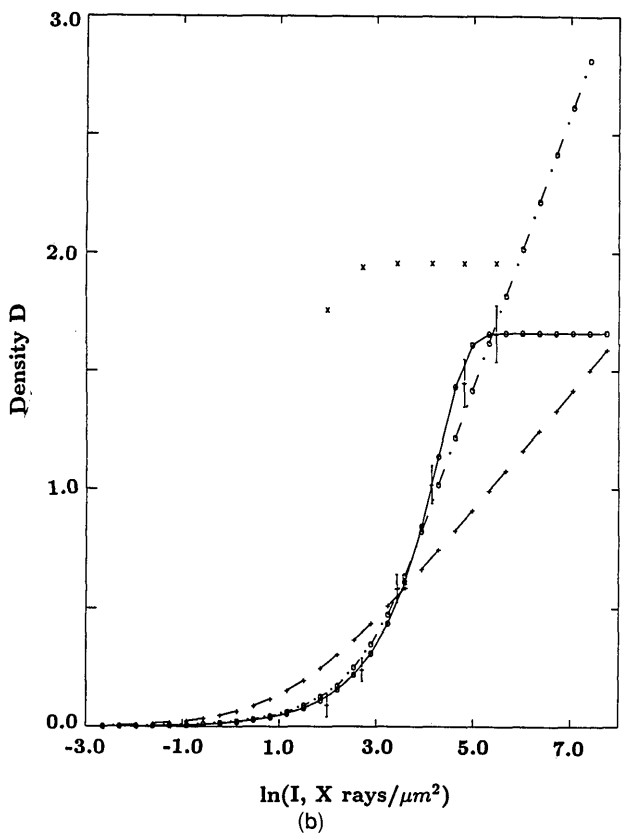
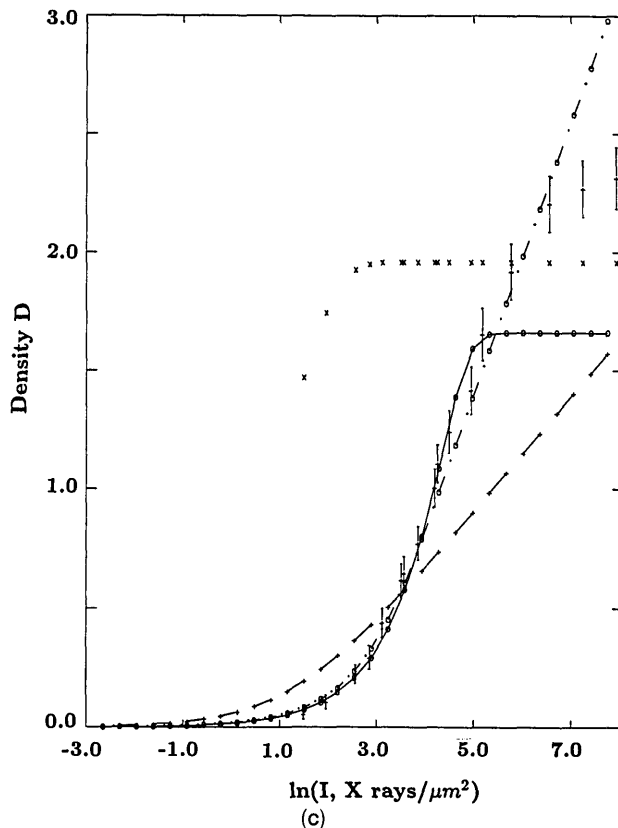
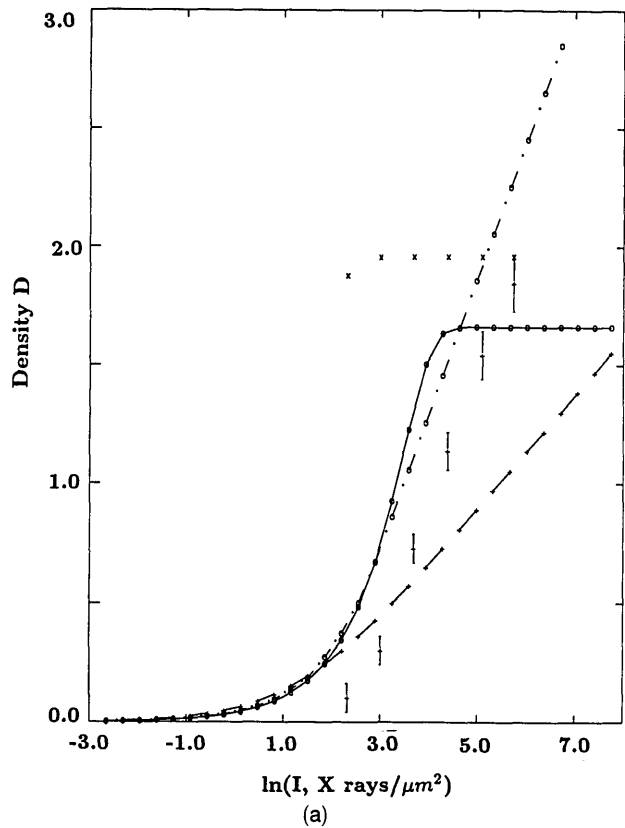


Fig. 13. (continued.)

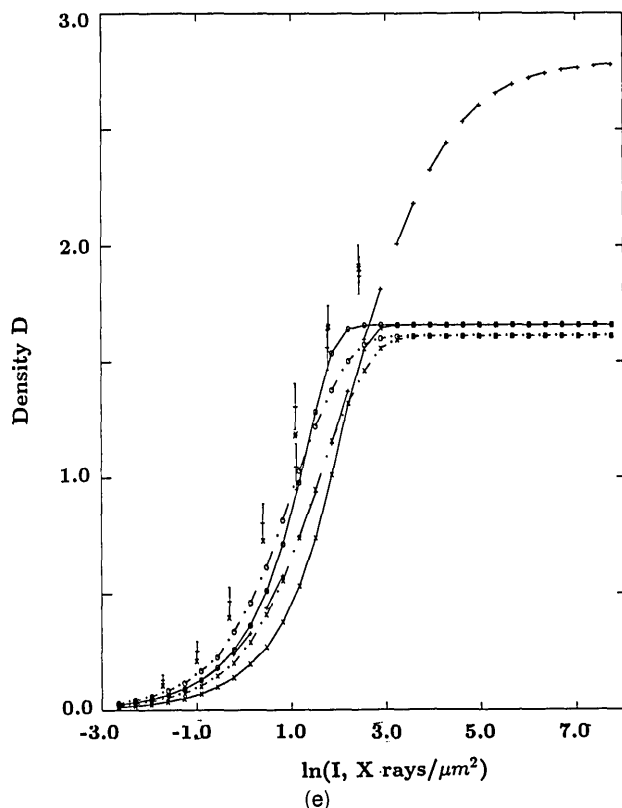


Fig. 13.  $D$ - $\ln I$  relations for 101 emulsion and (a) 5.254-eV, (b) 9.508-eV, (c) 10.332-eV, (d) 16.869-eV, and (e) 524.9-eV radiation with thin-emulsion ( $\times$ ), rough [Eq. (25b) ( $\text{O}\cdot\text{---}\text{O}$ )], thick-emulsion (Ref. 8,  $+ \text{---} +$ ), and optimized Eq. (25c) ( $\text{---}\text{O}\text{---}$ ) models from Table 5. Data ( $+$ ) are compared with modeling. In (d) and (e) the corresponding smooth models are presented ( $\times\text{---}\times$ ,  $\text{---}\times\text{---}$ ) to show the similarity above 200 eV and their inadequacy below this energy.

tively, and may either approach the correct value or become a factor of 25 too large for low energies, depending on the emulsion type. This [Fig. 11(a)] relates to normal incidence; the effect of the angle (which is not applicable in the earlier formula) may increase this by factors of 5, reduce it by factors of 3 for low-energy photons and smooth emulsions, or reduce it by factors of 2 for low-energy photons and rough emulsions, while having little effect above  $\sim 4$  keV.

The single dominant effect of angle on the  $D$ - $I$  relation is (usually) given by Eq. (5) or the equivalent  $(\sin \theta)/\mu'$  ratio with either the empirical  $d_0$  correction in Eq. (25b) or the initial logarithm offset of Eqs. (25a) and (25c). Hence the variation in  $\mu'$  by 15% corresponds directly to the variation in the density scaling at low and intermediate exposure by the same magnitude. This asymptotic variation is discussed in Section 16. The effect of the variation in  $J$  or  $\beta$  leads to a scaling error of the same factor for low and intermediate exposures, which cancel in the saturation limit, and with a scaled logarithmic offset in the linear regime.

Since these effects can be mimicked by empirical parameters  $a$  and  $b$  (or similar errors in  $\sigma$  and  $M_0S$ ), a semiempirical function such as Eq. (6) fitted over (narrow) ranges of density and energy may be quite accurate. However, the parameters derived from such a procedure may bear little relation to the intended physical quantities, systematic deviations may be expected near the limits of the ranges fitted, and extrapolation from individual energies and densi-

ties to other regimes may give large errors. In particular the parameters derived should not be taken as constants of the emulsion type. Conversely, the parameters derived herein may more accurately be considered to be constant for a given emulsion.

## 20. Criticism of Current Model Assumptions and Conclusions

The current models of Eqs. (25a)-(25c) provide accurate and useful predictions of density as a function of intensity for the extreme emulsions of DEF-392, 101-01, and 101-07 on a consistent basis across the range of density and energies between 9 eV and 20 keV. Existing data often cover only the linear  $D$ - $I$  region and the beginning of the  $D - \ln I$  regime because of densitometry limitations, so that simpler models can be applicable with distortion of values at higher densities. Corrections for background and diffuse/specular density conversion must be made with care, especially at high and low densities. Further tests with specialized densitometry may discriminate between these and other models.

Current formulations investigate the integral form for the  $D$ - $I$  relation, presenting effects of low-density, low-coverage, and high-energy assumptions. The variation with incident angle and energy is given in a more self-consistent way, assuming uniform diameters and spheres of grains. Asphericity and nonuniform diameters are assumed to be negligible for most standard modern emulsions.

The formulations treat deep layers accurately and

differ in the evaluation of density contributions for the first layers, especially for low energies. The major difficulty with this contribution is the correlated coverage and attenuation coefficients with depth and exposure. This cannot be readily developed within an integral formalism. The problem is addressed in the subsequent paper.

Consequent difficulty arises in higher-density regimes and, because of slight distortion of parameters, with extrapolation to widely differing energies. Despite this, these models may be fitted to data over a given energy and density range and may be expected to be valid over a considerably wider range.

The author thanks Shell Australia, the Hasselblad Foundation, and the Draper's Company for support of this research and St. Anne's College, Oxford, for a Junior Research Fellowship covering part of the period of research. The author acknowledges the assistance and support of J. D. Silver, D. D. Dietrich, and J. M. Laming.

## References

1. R. A. Armistead, "Calibration of Kodak fine grain positive and no-screen film in the 4–52 keV x-ray range," *Rev. Sci. Instrum.* **45**, 996–1000 (1974).
2. G. Barnea and A. Ginzburg, "High energy x-ray film response and the intensifying action of metal screens," *IEEE Trans. Nucl. Sci.* **NS-34**, 1580–1585 (1987).
3. D. B. Brown, J. W. Criss, and L. S. Birks, "Sensitivity of x-ray films. I. A model for sensitivity in the 1–100 keV region," *J. Appl. Phys.* **47**, 3722–3731 (1976).
4. C. M. Dozier, J. V. Gilfrich, and L. S. Birks, "Qualitative calibration of x-ray film response in the 5 keV to 1.3 MeV region," *Appl. Opt.* **6**, 2136–2139 (1967).
5. C. M. Dozier, D. B. Brown, L. S. Birks, P. B. Lyons, and R. F. Benjamin, "Sensitivity of x-ray film. II. Kodak no-screen film in the 1–100 keV region," *J. Appl. Phys.* **47**, 3732–3739 (1976).
6. B. L. Henke, S. L. Kwok, J. Y. Uejio, H. T. Yamada, and G. C. Young, "Low-energy x-ray response of photographic films. I. Mathematical models," *J. Opt. Soc. Am.* **B1**, 818–827 (1984).
7. B. L. Henke, F. G. Fujiwara, M. A. Tester, C. H. Dittmore, and M. A. Palmer, "Low-energy x-ray response of photographic films. II. Experimental characterization," *J. Opt. Soc. Am.* **B 1**, 828–849 (1984).
8. B. L. Henke, J. Y. Uejio, G. F. Stone, C. H. Dittmore, and F. G. Fujiwara, "High-energy x-ray response of photographic films: models and measurement," *J. Opt. Soc. Am.* **B 3**, 1540–1550 (1986).
9. W. C. Phillips and G. N. Phillips, Jr., "Two new x-ray films: conditions for optimum development and calibration of response," *J. Appl. Crystallogr.* **18**, 3–7 (1985).
10. A. Poquérusse, "Réponse du film SB aux rayons X de 0,1 à 10 keV," *Rev. Phys. Appl.* **23**, 963–969 (1988).
11. P. D. Rockett, C. R. Bird, C. J. Hailey, D. Sullivan, D. B. Brown, and P. G. Burkhalter, "X-ray calibration of Kodak direct exposure film," *Appl. Opt.* **24**, 2536–2542 (1985).
12. W. M. Burton, A. T. Hatter, and A. Ridgeley, "Photographic sensitivity measurements in the vacuum ultraviolet," *Appl. Opt.* **12**, 1851–1857 (1973).
13. C. T. Chantler, "Beam-foil spectroscopy of highly-ionized atoms, precision measurements of hydrogenic Lamb shifts and x-ray diffraction of crystals," D.Phil. thesis (Oxford University, Oxford, 1990).
14. J. M. Laming, "A differential measurement of the ground state Lamb shift in hydrogenic germanium,  $\text{Ge}^{31+}$ ," D.Phil. thesis (Oxford University, Oxford, 1988).
15. J. M. Laming, C. T. Chantler, J. D. Silver, D. D. Dietrich, E. C. Finch, P. H. Mokler, and S. D. Rosner, "A differential measurement of the ground state Lamb shift in hydrogenic germanium,  $\text{Ge}^{31+}$ ," *Nucl. Instrum. Methods B* **31**, 21–23 (1988).
16. C. E. K. Mees, *The Theory of the Photographic Process* (Macmillan, New York, 1946).
17. G. M. B. Dobson, I. O. Griffith, and D. N. Harrison, *Photographic Photometry* (Oxford U. Press, Oxford, 1926).
18. B. L. Henke and M. A. Tester, "Techniques of low energy x-ray spectroscopy (0.1–2-keV region)," in *23rd Annual Denver Conference on Applications of X-ray Analysis, August 7–9, 1974*, W. L. Pickles, ed., Vol. 18 of *Advances in X-Ray Analysis* (Plenum, New York, 1975), pp. 76–106.
19. B. L. Henke, P. Lee, T. J. Tanaka, R. L. Shimabukuro, and B. K. Fujikawa, "Low-energy x-ray interaction coefficients: photoabsorption, scattering, and reflection,  $E = 100\text{--}2000$  eV,  $Z = 1\text{--}94$ ," *At. Data Nucl. Data Tables* **27**, 1–144 (1982).
20. R. F. Reilman and S. T. Manson, "Photoabsorption cross sections for positive atomic ions with  $Z \leq 30$ ," *Astron. J. Suppl. Ser.* **40**, 815–880 (1979).
21. W. J. Veigele, "Photon cross sections from 0.1 keV to 1 MeV for elements  $Z = 1$  to  $Z = 94$ ," *At. Data Tables* **5**, 51–111 (1973).
22. L. Pages, E. Bertel, H. Joffre, and L. Sklavenitis, "Energy loss, range and bremsstrahlung yield for 10-keV to 100-MeV electrons in various elements and chemical compounds," *At. Data Tables* **4**, 1–127 (1972), especially pp. 92 and 109.
23. A. P. H. Trivelli and S. E. Sheppard, *The Silver Bromide Grain of Photographic Emulsions* (Van Nostrand, New York, 1921).
24. C. T. Chantler, J. D. Silver, and D. D. Dietrich, "Photographic response to x-ray irradiation. III. Photographic linearization of beam-foil spectra," *Appl. Opt.* **32**, 2411–2421 (1993).